

Optimal robust trajectory tracking control of a X-rudder AUV with velocity sensor failures and uncertainties

Yingkai Xia^a, Kan Xu^b, Wenjin Wang^a, Guohua Xu^{a,*}, Xianbo Xiang^a, Ye Li^c

^a School of Naval Architecture and Ocean Engineering, Huazhong University of Science and Technology, Wuhan, 430074, China

^b Wuhan Second Ship Design and Research Institute, Wuhan, 430205, China

^c School of Naval Architecture, Ocean & Civil Engineering, Shanghai Jiao Tong University, Shanghai, 200240, China

ARTICLE INFO

Keywords:

X-rudder AUV
Trajectory tracking control
Velocity sensor failures
Robust disturbance rejection control
Multi-objective optimal rudder allocation

ABSTRACT

This paper presents an optimal robust control method for trajectory tracking of a X-rudder autonomous underwater vehicle (AUV) subjects to velocity sensor failures and uncertainties. Two reduced-order extended state observers (ESOs) are designed to estimate the surge and heave velocities, and the estimated values are used to replace all the linear velocity-related parameters in controller design, which helps releasing the requirements of linear velocities measurement and makes the controller robust against linear velocity sensor failures. In kinematics control loop, line-of-sight (LOS) guidance law and Lyapunov-based control are employed, and the unknown attack angle is calculated based on the estimated linear velocities. In dynamics control loop, a robust disturbance rejection control law is constructed using disturbance observers and modified terminal sliding mode control. Moreover, a multi-objective optimization method is proposed to achieve X-rudder allocation, which is not only energy efficient but also robust against rudder failures, and helps tackling the rudder input saturation problem at the same time. Finally, comparative numerical simulations are provided to demonstrate the robustness and effectiveness of the proposed approach.

1. Introduction

Due to the depletion of land resources, marine development has received more and more attention, and various underwater equipment have been developed in the past few decades. Autonomous underwater vehicle is one of the most widely used underwater equipment, which has played an increasingly important role in all kinds of submerged applications, such as underwater intervention (Zhang et al., 2015), monitoring and inspection (Zhang et al., 2018a), target tracking (Shojaei and Dolatshahi, 2017), and oceanographic surveys (Wynn et al., 2014), etc.

To better accomplish the afore-mentioned submerged tasks, the following two basic ideas have been applied to improve the vehicle's performance: 1) Design effective control systems to steer the AUVs accurately and reliably in the harsh marine environment; 2) Design new actuators such as rudders, thrusters, etc. to improve the vehicle's capability. With the thought of second kind, various kinds of rudders have been applied to AUV to improve the maneuverability, such as cross rudder, H type rudder, and X type rudder (Zhang et al., 2017), etc. Compared with traditional cross rudder AUV, the X-rudder AUV has much better maneuverability and flexibility since the four rudders can

be operated independently. However, the control of the X-rudder AUV is more complicated than cross rudder AUV, and is not often studied in the existing literatures. For this reason, trajectory tracking control of a X-rudder AUV will be discussed in this paper.

Trajectory tracking control of marine vehicles has been widely studied in recent years (Xia et al., 2019a; Yu et al., 2019a; Shen et al., 2018; Zhang et al., 2019; Al Makdah et al., 2019). In Qiao et al. (2017), three exponentially convergent robust controllers, namely, the min-max type controller, the saturation type controller, and the smooth transition type controller were proposed to drive an AUV to track a predefined trajectory. In von Ellenrieder (2019), an n-degree of freedom nonlinear control law was proposed for the trajectory tracking of marine vehicles that operate in the presence of unknown time-varying disturbances, input saturation and actuator rate limits, using a disturbance observer and nonlinear dynamic surface control. An adaptive ILOS guidance law was proposed for unmanned MSVs in Zheng and Sun (2016), which introduced RBFNN to deal with the time-varying ocean currents. In Yu et al. (2018), line-of-sight (LOS) guidance was built for the robust magnetic tracking of subsea cable by an AUV, in the presence of sensor noise and ocean currents. In Miao et al. (2017), an improved compound

* Corresponding author.

E-mail address: hustxu@vip.sina.com (G. Xu).

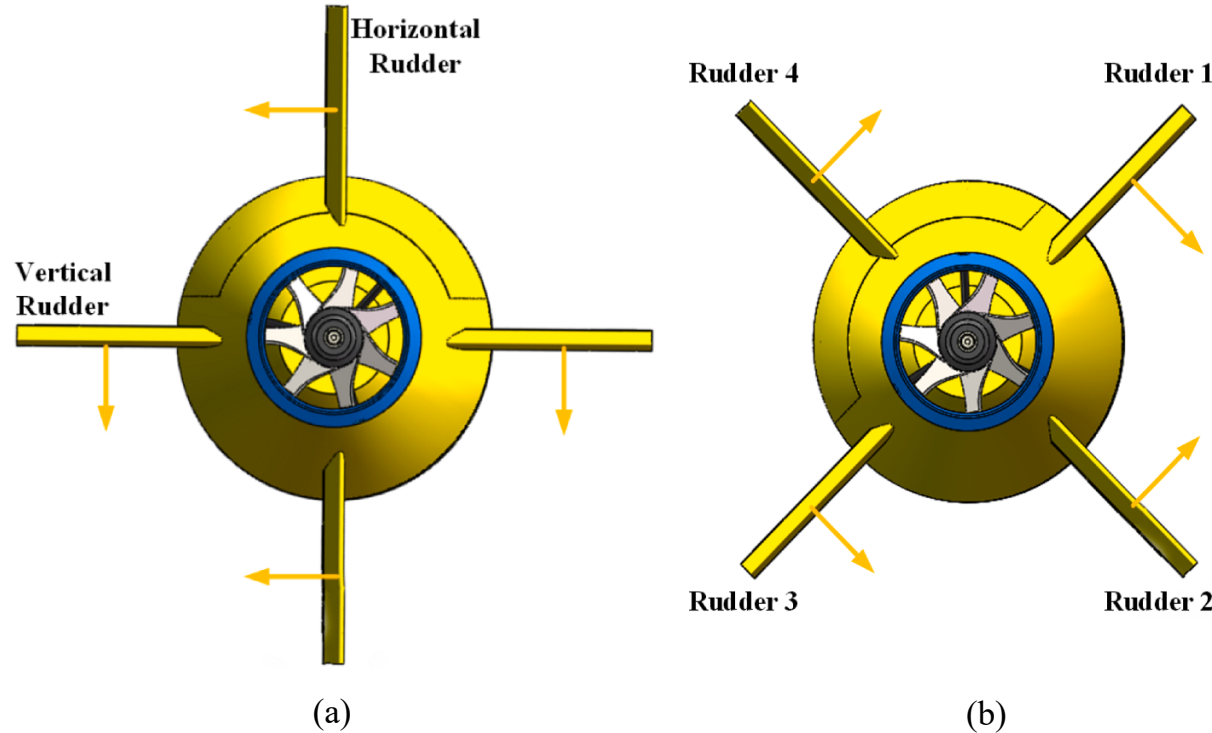


Fig. 1. Layout comparison of the Cross-rudder and X-rudder. (a) Cross-rudder; (b) X-rudder.

line-of-sight (CLOS) guidance law was proposed for path following control of AUV, which can estimate the unknown sideslip angle and compensate for the effects of time-varying ocean currents. In Chen et al. (2019), an adaptive trajectory tracking control algorithm was proposed with guaranteed transient performance, which employed neural networks to approximate the unknown external disturbances and uncertain hydrodynamics.

Most of the above studies are based on the assumption that all the motion states of AUV are measurable. However, sensor failures may occur to AUV considering the complex underwater environment. In these cases, the conventional control methods may not work. State observer based control methods can provide effective solutions for such conditions. Yu et al. (2019b) proposed an improved extended state observer-based line-of-sight (ELOS) guidance law, which estimated the surge and sway linear velocities and compensated for the unmeasured side-slip angle, but the estimated velocities were only utilized in kinematics control and not applied in dynamics control. An output feedback path-following control method was proposed in Peng and Wang (2018) for under-actuated autonomous underwater vehicles moving in a vertical plane without using surge, heave, and pitch velocities. In Li et al. (2019), a finite-time extended state observer based fault tolerant output feedback control was proposed for the rigid spacecraft attitude control system without the angular velocity measurements, in the presence of external disturbances and actuator failures. In Liu et al. (2019), the state recovery and disturbance estimation problems of unmanned surface vehicles were addressed in the presence of unknown disturbances as well as unmeasured surge, sway, and yaw velocities. Motivated by the existing methods, extended state observers (ESOs) are proposed to estimate the surge and heave velocities in this paper, and the estimated values are used to replace all the velocity-related parameters in controller design. Hence, the trajectory tracking missions can be completed without requirements of linear velocity measurement.

Complex unknown external disturbance is an important issue of trajectory tracking, which could affect the model accuracy and degrade the closed-loop system performance (Wang et al., 2013, 2018). To solve this problem, the control system should have good robustness. The commonly used robust control methods include but not limited to sliding mode control (Guo et al., 2019), H-infinity control (Zhang et al., 2018b), model predictive control (Li and Yan, 2017), neural network control (Xia et al., 2019b), optimal control (Li et al., 2018), Multi-agent

(Xiao et al., 2018), etc. Of all the robust control methods, sliding mode control is a widely used robust control technique, which has shown excellent tracking performance due to its robustness against the uncertainties and disturbances (Van, 2019). In Qiao and Zhang (2017), an adaptive non-singular integral terminal sliding mode control (ANITSMC) scheme was proposed for trajectory tracking of autonomous underwater vehicles (AUVs) with dynamics uncertainties and time-varying external disturbances. In Xu et al. (2015), sliding mode control and backstepping technique were combined to design a robust trajectory tracking controller, for an AUV with parameter uncertainties and external disturbances. Qiao and Zhang (2019) proposed an adaptive second-order fast nonsingular terminal sliding mode control (ASOFNTSMC) scheme for the trajectory tracking of fully actuated autonomous underwater vehicles (AUVs) in the presence of dynamic uncertainties and time-varying external disturbances. However, chattering problems are often encountered for sliding mode control. To guarantee control robustness and avoid chattering, a robust disturbance rejection control law is constructed in this paper based on disturbance observers and modified terminal sliding mode control.

Actuator dynamics is another technical challenge for trajectory tracking control. The commonly considered actuator dynamics include input saturation, input delay, etc., which may influence the stability of the control system and even make the entire system unstable. Many efforts have been made to tackle these problems in recent years. An anti-windup compensator was proposed in Cui et al. (2016) to solve the problem of attitude control subjected to actuator saturation. Novel auxiliary systems were proposed in Chu et al. (2018) to deal with the input saturation, based on which, an adaptive fuzzy sliding mode controller was developed for the diving control of AUV. To eliminate the control input nonlinearities, adaptive neural network control was proposed in Cui et al. (2017) for AUVs using reinforcement learning. In Peng et al. (2019), a reference governor was used for generating the optimal reference signals within the state and input constraints, based on which, the guidance loop and the control loop were bridged. In Sarhadi et al. (2016), an adaptive autopilot was presented for the pitch and yaw channels of an AUV in presence of input saturations, which employed model reference adaptive control with integral state feedback and anti-windup compensator. However, most of the above studies are designed for the cross-rudder AUV, which cannot solve the single-input and multi-output (SIMO) rudder angle distribution problem faced by the

X-rudder AUV. To solve this problem, a multi-objective optimization method is proposed in this paper, which considers the problem of torque distribution, energy consumption, input saturation, and can handle rudder failures.

Motivated by the afore-mentioned considerations, this paper proposes an optimal robust trajectory tracking controller for a X-rudder AUV in the presence of velocity sensor failure and uncertainties. The main contributions are summarized as follows:

- (1) Two reduced-order extended state observers (ESOs) are proposed to estimate the surge and heave velocities, and the estimated values are used to replace all the velocity-related parameters in controller design. Hence, the trajectory tracking missions can be completed in presence of velocity sensor failures. Compared with conventional trajectory tracking controller, the proposed method can achieve trajectory tracking missions without using the measured linear velocities.
- (2) An optimal robust disturbance rejection control law is designed for dynamics control, which solves the problem of unknown compound disturbances by disturbance observers, improves the system robustness and asymptotic convergence by employing modified terminal sliding mode control, and achieves rudder allocation by multi-objective optimization method. Compared with conventional disturbance observer method, the proposed method utilizes the estimated velocities rather than the measured

independent control property and diagonal arrangement, the X-rudder AUV has better ability to resist the rudder stuck, and also reduces the serious damage caused by rudder stuck; 5) Lower noise: The layout of X rudder helps reduce interference between the rudder and propeller, thus reducing the noise. However, the control of the X-rudder AUV is more complicated than Cross-rudder AUV, since the direction of control surface of X-rudder is inconsistent with the moving direction of AUV, which increases the cross-coupling and the AUV can't be intuitively controlled. Usually the rudder force and torque of the desired direction are calculated first, then SIMO rudder angle distribution problem will be solved to obtain the rudder angles. To tackle the above problem, the X-rudder dynamics model will be studied in this section.

Following standard practice, the kinematic and dynamic model of the AUV in vertical plane can be described by the motion components in surge, heave, and pitch degrees of freedom.

The kinematics model of AUV take the following form:

$$\begin{cases} \dot{x} = u \cos \theta + w \sin \theta \\ \dot{z} = -u \sin \theta + w \cos \theta \\ \dot{\theta} = q \end{cases} \quad (1)$$

*θ_i朝向
u和x的夹角*

where $[x, z, \theta]^T$ denote the position and orientation vectors of the AUV in inertial reference frame, u , w , and q are the surge, heave, and pitch angular velocities.

Neglecting the motions in sway, yaw, and roll directions, the 3-DOF dynamics model of AUV in vertical plane is simplified as

$$\begin{cases} (m - X_u)\dot{u} = -(W - B)\sin \theta - mwq + mx_g q^2 + X_{u|u}|u| + X_{wq}wq + X_{qq}q^2 + X_T + D_u \\ (m - Z_w)\dot{w} = (W - B)\cos \theta + muq + mz_g q^2 + Z_{w|w}|w| + Z_{q|q}|q| + Z_{uq}uq + Z_{uw}uw + \tau_w + D_w \\ (I_{yy} - M_q)\dot{q} = -(z_g W - z_b B)\sin \theta - (x_g W - x_b B)\cos \theta - mz_g wq - mx_g uq + M_{w|w}|w| + M_{q|q}|q| \\ \quad + M_{uq}uq + M_{uw}uw + \tau_q + D_q \end{cases} \quad (2)$$

values. Besides, the proposed multi-objective optimization method is not only energy efficient but also robust against rudder failures.

The remainder of this paper is organized as follows. Section 2 presents the X-rudder AUV models, trajectory tracking mission, and control problem formulation. Section 3 proposes the optimal robust trajectory tracking control scheme, and presents the detailed deriving process of kinematics and dynamics controller. Section 4 validates the previous analysis and design through simulation cases and discussions. Section 5 demonstrates the conclusions of this work.

2. Problem formulation

2.1. X-rudder AUV model

In this paper, a X-rudder AUV will be studied, which has a special control surface layout, as shown in Fig. 1. Compared with traditional Cross-rudder AUV, X-rudder AUV has following advantages: 1) Higher safety: The X-rudder can be arranged within the vehicle's baseline, thus avoiding unexpected collisions between the rudders and underwater obstacles; 2) Better maneuverability: The X-rudder AUV has better hydrodynamic performance and stability in both horizontal and vertical planes, and the rolling motion can be controlled; 3) Better rudder efficiency: The X rudder adopts a diagonal arrangement to obtain the maximum extension length, which helps achieving large aspect ratio and high rudder efficiency; 4) Stronger anti-sinking ability: Due to the

where m is the mass of vehicle, W is the vehicle's weight, B is the vehicle's buoyancy, (x_g, z_g) is the position of vehicle's gravity center in the body-fixed frame, (x_b, z_b) is the position of vehicle's buoyancy center in the body-fixed frame, I_{yy} is the moment of inertia of the vehicle about y-axis of the body-fixed frame. X_* , Z_* , and M_* are the vehicle's hydrodynamics coefficients. X_T is the propeller thrust force along the vehicle's

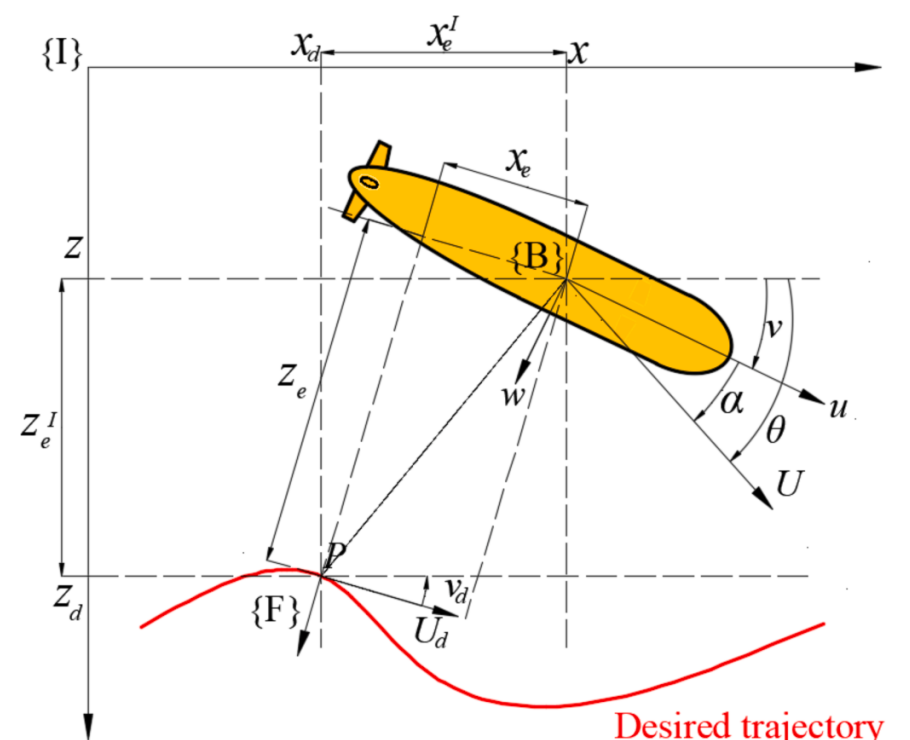


Fig. 2. Trajectory tracking mission in vertical plane.

surge motion, τ_w and τ_q are the rudder force and torque along the vehicle's heave motion and pitch motion respectively. D_u , D_w , and D_q denote unknown compound environmental disturbances with unknown upper bounds.

To facilitate the controller design, the dynamics model of AUV in vertical plane is rewritten as

$$\begin{cases} \dot{u} = f_u(u, w, q) + g_u X_T + d_u \\ \dot{w} = f_w(u, w, q) + g_w \tau_w + d_w \\ \dot{q} = f_q(u, w, q) + g_q \tau_q + d_q \end{cases} \quad (3)$$

where

$$\begin{aligned} f_u(u, w, q) &= \left(- (W - B) \sin \theta - mwq + mx_g q^2 + X_{u|u} |u| u + X_{wq} wq + X_{qq} q^2 \right) / (m - X_u) \\ g_u &= 1 / (m - X_u) \\ d_u &= D_u / (m - X_u) \\ f_w(u, w, q) &= \left((W - B) \cos \theta + muq + mz_g q^2 + Z_{w|w} |w| w + Z_{q|q} |q| q + Z_{uq} uq + Z_{uw} uw \right) / (m - Z_w) \\ g_w &= 1 / (m - Z_w) \\ d_w &= D_w / (m - Z_w) \\ f_q(u, w, q) &= \left(-(z_g W - z_b B) \sin \theta - (x_g W - x_b B) \cos \theta - mz_g wq - mx_g uq \right) / (I_{yy} - M_{\dot{q}}) \\ &\quad + M_{w|w} |w| w + M_{q|q} |q| q + M_{uq} uq + M_{uw} uw \\ g_q &= 1 / (I_{yy} - M_{\dot{q}}) \\ d_q &= D_q / (I_{yy} - M_{\dot{q}}) \end{aligned}$$

Moreover, the rudder force and torque of the X-rudder AUV can be expressed as

$$\begin{cases} \tau_w = Z_{uu\delta_1} u^2 \delta_1 + Z_{uu\delta_2} u^2 \delta_2 + Z_{uu\delta_3} u^2 \delta_3 + Z_{uu\delta_4} u^2 \delta_4 \\ \tau_q = M_{uu\delta_1} u^2 \delta_1 + M_{uu\delta_2} u^2 \delta_2 + M_{uu\delta_3} u^2 \delta_3 + M_{uu\delta_4} u^2 \delta_4 \end{cases} \quad (4)$$

where Z_* and M_* are the hydrodynamics coefficients, $\delta_1, \delta_2, \delta_3$, and δ_4 are the four rudder angles of the X-rudder AUV.

Remark 1. For marine vehicles, there exists inherent actuator saturation (Naik and Singh, 2007; Zheng et al., 2017). Therefore, the propeller thrust and rudder angles of the AUV discussed here should be bounded, viz. $|X_T| \leq \bar{X}_T$ and $|\delta_*| \leq \bar{\delta}$, where \bar{X}_T is a known positive constant, δ_* represent $\delta_1, \delta_2, \delta_3$, and δ_4 , $\bar{\delta}$ is a known positive constant.

Remark 2. Due to the actuator saturation and energy limitation, the velocities and their time-derivatives should be bounded, viz. $|u| \leq \bar{u}$, $|w| \leq \bar{w}$, $|\dot{u}| \leq \bar{\dot{u}}$, $|\dot{w}| \leq \bar{\dot{w}}$.

2.2. Trajectory tracking mission

As shown in Fig. 2, the vehicle is required to track a desired trajectory in the vertical plane, where $\{I\}$, $\{B\}$, and $\{F\}$ designate the inertial reference frame, the body-fixed frame, and the Frenet-Serret frame, respectively. P is a moving point on the trajectory to be tracked. Associated with P on the desired trajectory, $\{F\}$ is built, and the axes of which are tangent and normal to the trajectory.

Let $(x, z)^T$ and $(x_d, z_d)^T$ be the AUV position and target position in $\{I\}$ respectively. Then, the trajectory tracking errors built in $\{I\}$ can be described as

$$\begin{cases} x_e^I = x - x_d \\ z_e^I = z - z_d \\ v_e^I = v - v_d \end{cases} \quad (5)$$

*V: X轴的偏差
代表 AUV 的姿态*

where $v = \theta - \alpha$, $\alpha = \arctan(w/u)$, $v_d = \arctan(-\dot{z}_d/\dot{x}_d)$.

Subsequently, the trajectory tracking error vector built in $\{F\}$ is derived as

$$\begin{bmatrix} x_e \\ z_e \\ v_e \end{bmatrix} = \begin{bmatrix} \cos v_d & -\sin v_d & 0 \\ \sin v_d & \cos v_d & 0 \\ 0 & 0 & 1 \end{bmatrix} \begin{bmatrix} x_e^I \\ z_e^I \\ v_e^I \end{bmatrix} \quad (6)$$

Differentiating (6) and utilizing (1) yields

$$\begin{aligned} \dot{x}_e &= (\dot{x} - \dot{x}_d) \cos v_d - (x - x_d) \dot{v}_d \sin v_d - (z - z_d) \dot{v}_d \cos v_d \\ &= (u \cos \theta + w \sin \theta - \dot{x}_d) \cos v_d - \dot{v}_d (x - x_d) \sin v_d \\ &\quad - (-u \sin \theta + w \cos \theta - \dot{z}_d) \sin v_d - \dot{v}_d (z - z_d) \cos v_d \\ &= u \cos(\theta - v_d) + w \sin(\theta - v_d) - U_d (1 + \kappa z_e) \end{aligned} \quad (7)$$

$$\begin{aligned} \dot{z}_e &= (\dot{x} - \dot{x}_d) \sin v_d + (x - x_d) \dot{v}_d \cos v_d + (\dot{z} - \dot{z}_d) \cos v_d - (z - z_d) \dot{v}_d \sin v_d \\ &= (u \cos \theta + w \sin \theta - \dot{x}_d) \sin v_d + \dot{v}_d (x - x_d) \cos v_d \\ &\quad + (-u \sin \theta + w \cos \theta - \dot{z}_d) \cos v_d - \dot{v}_d (z - z_d) \sin v_d \\ &= -u \sin(\theta - v_d) + w \cos(\theta - v_d) + \kappa U_d x_e \end{aligned} \quad (8)$$

where $U_d = \sqrt{\dot{x}_d^2 + \dot{z}_d^2}$ is the velocity of the point P on the desired trajectory, κ is the curvature of the point P on the desired trajectory, and $\kappa = \dot{v}_d/U_d$.

Hence, the trajectory tracking error dynamics can be expressed as

$$\begin{bmatrix} \dot{x}_e \\ \dot{z}_e \\ \dot{v}_e \end{bmatrix} = \begin{bmatrix} u \cos(\theta - v_d) + w \sin(\theta - v_d) - U_d (1 + \kappa z_e) \\ -u \sin(\theta - v_d) + w \cos(\theta - v_d) + \kappa U_d x_e \\ q - \dot{\alpha} - \dot{v}_d \end{bmatrix} \quad (9)$$

2.3. Problem formulation

Our objective is to develop a controller to regulate the AUV to track the desired trajectory in the vertical plane, regardless of velocity sensor failures, unknown external disturbances, and complex actuator dynamics. The objective can be divided into two control problems, as shown below.

- (1) **Kinematics control:** Given a desired trajectory and the trajectory tracking error model (7–8), derive an effective kinematics control law to generate the required surge velocity u_d and pitch angular velocity q_d , so that the trajectory tracking error vectors can converge to zero as t goes to ∞ .
- (2) **Dynamics control:** Given the desired surge velocity u_d and pitch angular velocity q_d , and the dynamics model (3–4), derive effective dynamics control laws to generate the control input $(X_T, \delta_1, \delta_2, \delta_3, \delta_4)$, so that the tracking errors $u - u_d$ and $q - q_d$ can converge to zero as t goes to ∞ .

To facilitate the trajectory tracking controller design, following assumptions are required:

Assumption 1. The predefined trajectory are finite, such that x_d, y_d , \dot{x}_d , and \dot{y}_d are bounded.

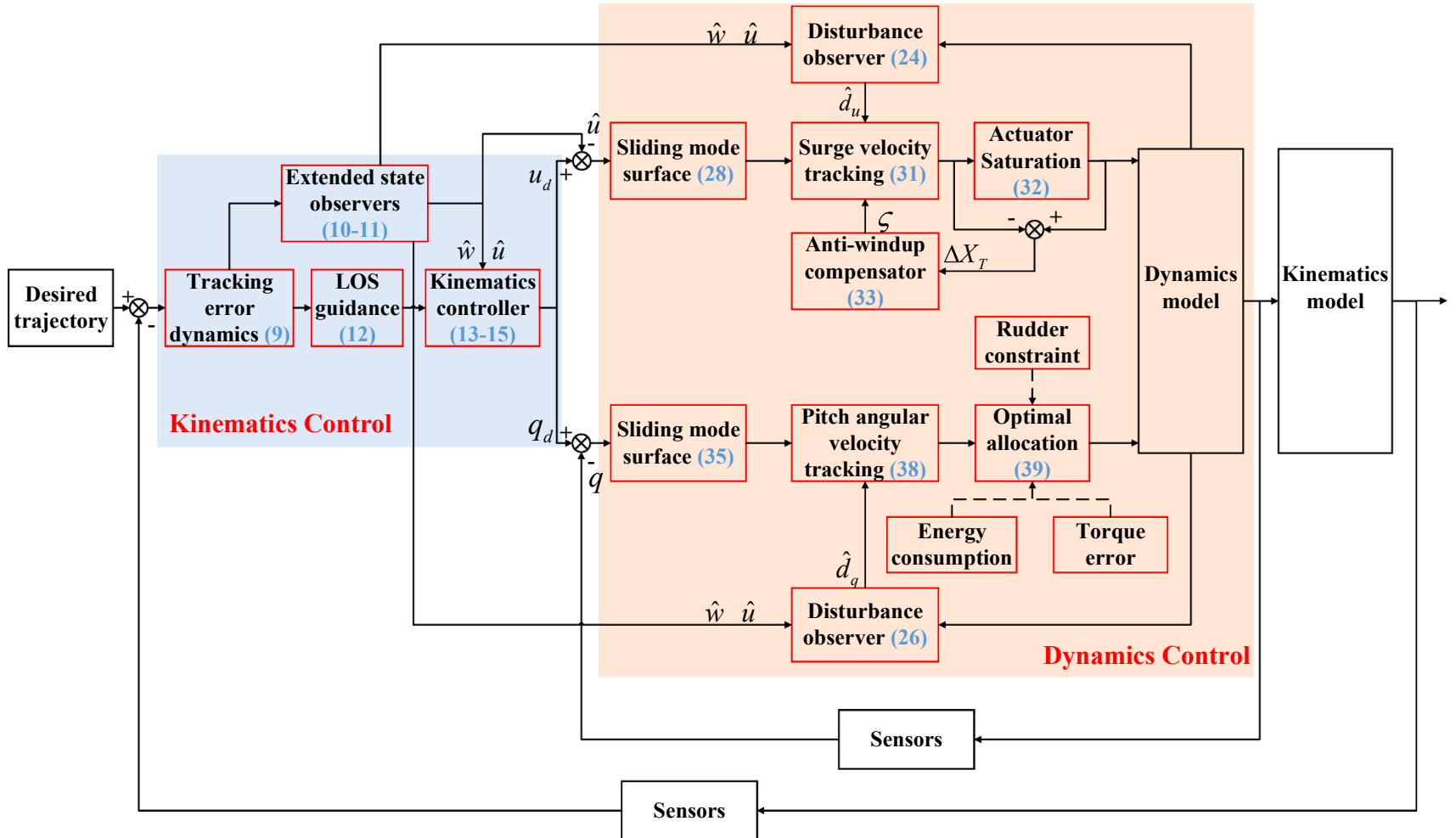


Fig. 3. The proposed trajectory tracking control scheme.

Assumption 2. The unknown environmental disturbances and their time-derivatives are assumed to be bounded, viz. $|d_u| \leq \bar{d}_u$, $|\dot{d}_u| \leq \bar{\bar{d}}_u$, $|d_w| \leq \bar{d}_w$, $|\dot{d}_w| \leq \bar{\bar{d}}_w$, $|d_q| \leq \bar{d}_q$, and $|\dot{d}_q| \leq \bar{\bar{d}}_q$, where \bar{d}_u , \bar{d}_w , \bar{d}_q , $\bar{\bar{d}}_u$, $\bar{\bar{d}}_w$, and $\bar{\bar{d}}_q$ are positive constants.

Assumption 3. The position vector (x, z) and the pitch angle θ are measurable, whereas the linear velocities u and w are unmeasurable due to the linear velocity sensor failures.

3. Controller design

无速度传感器
无速度传感器

As analyzed before, the X-rudder AUV discussed in this paper subjects to coupled nonlinearities, uncertainties, complex actuator dynamics, and velocity sensor failures. In order to achieve satisfying trajectory tracking in vertical plane, the proposed controller needs to achieve not only good kinematics guidance without linear velocities measurements, but also accurate and robust dynamics control against the highly coupled nonlinearities, unknown disturbances, and complex X-rudder dynamics. Considering the aforementioned problems, an optimal robust trajectory tracking controller is proposed in this section, the control architecture of which is shown in Fig. 3.

The proposed trajectory tracking control law is divided into two parts: kinematics loop and dynamics loop. ESOs are designed to estimate the linear velocities, and the estimated values are used to replace all the velocity-related parameters in controller design. Hence, the trajectory tracking missions can be completed without using the measured linear velocities. LOS guidance law and backstepping kinematics control law are utilized in kinematics loop. To address the system robustness against unknown uncertainties, disturbance observer based terminal sliding mode control is utilized in dynamics loop with modified sliding mode surfaces and reaching laws. The input saturation problem of propeller thrust is tackled by an anti-windup compensator. Moreover, a multi-objective optimization method is proposed to achieve rudder allocation, which is not only energy efficient but also robust against rudder failures, and helps tackling the rudder input saturation problem at the same time.

Compared with conventional trajectory tracking controller, the proposed controller has better engineering application value since it is not only robust against velocity sensor failures, but also energy efficient and robust against rudder failures, helps tackling the practical problems encountered in actual working environment. Besides, it is more suitable for X-rudder AUV control owing to the multi-objective optimization method utilized for rudder allocation.

3.1. Kinematics controller design

3.1.1. Linear velocity observer design

As illustrated in **Assumption 3**, the linear velocities u and w are unmeasurable. To facilitate the design of proposed controller, following two reduced-order extended state observers are utilized to estimate the surge and heave velocities (Yu et al., 2019b):

$$\begin{cases} \hat{u} = p_u + k_1 x_e \\ \dot{p}_u = -k_1 [\hat{u} \cos(\theta - v_d) + \hat{w} \sin(\theta - v_d) - U_d(1 + \kappa z_e)] \end{cases} \quad (10)$$

$$\begin{cases} \hat{w} = p_w + k_1 z_e \\ \dot{p}_w = -k_1 [-\hat{u} \sin(\theta - v_d) + \hat{w} \cos(\theta - v_d) + \kappa U_d x_e] \end{cases} \quad (11)$$

where \hat{u} and \hat{w} are the estimated values of u and w , p_u and p_w are the designed auxiliary variables, k_1 is the observer gain. Note that the two observers have the same observer gain.

3.1.2. LOS based kinematics controller design

To achieve kinematics guidance and control, following LOS guidance law is utilized:

$$v_{LOS} = \arctan\left(\frac{z_e}{\Delta}\right) \quad (12)$$

where Δ is a positive constant.

In addition, the desired surge velocity u_d and desired pitch angular velocity q_d are designed as:

根据 x_e 和 z_e 得出 u_d 和 q_d

$$\left\{ \begin{array}{l} u_d = (-k_2 x_e + U_d) \frac{\cos \alpha}{\cos v_e} \\ q_d = \dot{\alpha} + \kappa U_d + \dot{v}_{LOS} - k_3(v_e - v_{LOS}) + z_e \frac{f(v_e, v_{LOS})}{\cos \alpha} \end{array} \right. \quad (13)$$

手写注释：\sqrt{u_d^2 + 2d^2} \rightarrow 增益

where k_2 and k_3 are positive constants, and the function $f(v_e, v_{LOS})$ takes the following form:

$$f(v_e, v_{LOS}) = \begin{cases} \frac{\sin v_e}{v_e - v_{LOS}}, & v_e - v_{LOS} \neq 0 \\ 0, & v_e - v_{LOS} = 0 \end{cases} \quad (14)$$

It is seen that (13) involves a computation of α and $\dot{\alpha}$. Due to the failures of linear velocity sensors, the velocities u and w are unmeasurable. Hence, α and $\dot{\alpha}$ are calculated using the observed values as follows:

$$\begin{aligned} \dot{V}_1 &= -k_2 x_e^2 - z_e u \frac{\sin v_e}{\cos \alpha} + (v_e - v_{LOS}) \left[-k_3(v_e - v_{LOS}) + z_e \frac{f(v_e, v_{LOS})}{\cos \alpha} \right] \\ &+ k_1 \tilde{u} [-\tilde{u} \cos(\theta - v_d) - \tilde{w} \sin(\theta - v_d) - \dot{u}] + k_1 \tilde{w} [\tilde{u} \sin(\theta - v_d) - \tilde{w} \cos(\theta - v_d) - \dot{w}] \\ &= -k_2 x_e^2 - z_e u \frac{\sin v_e}{\cos \alpha} + (v_e - v_{LOS}) \left[-k_3(v_e - v_{LOS}) + z_e \frac{f(v_e, v_{LOS})}{\cos \alpha} \right] \\ &- k_1 \tilde{u}^2 \cos(\theta - v_d) - k_1 \tilde{w}^2 \cos(\theta - v_d) - k_1 \tilde{u} \dot{u} - k_1 \tilde{w} \dot{w} \\ &\leq -k_2 x_e^2 - z_e u \frac{\sin v_e}{\cos \alpha} + (v_e - v_{LOS}) \left[-k_3(v_e - v_{LOS}) + z_e \frac{f(v_e, v_{LOS})}{\cos \alpha} \right] \\ &- \left(k_1 \cos(\theta - v_d) - \frac{k_1}{2\varepsilon_1} \right) \tilde{u}^2 - \left(k_1 \cos(\theta - v_d) - \frac{k_1}{2\varepsilon_2} \right) \tilde{w}^2 + \frac{\varepsilon_1}{2} \dot{u}^2 + \frac{\varepsilon_2}{2} \dot{w}^2 \\ &= -k_2 x_e^2 - z_e u \frac{\sin v_e}{\cos \alpha} - k_3(v_e - v_{LOS})^2 + z_e \frac{f(v_e, v_{LOS})}{\cos \alpha} (v_e - v_{LOS}) \\ &- \left(k_1 \frac{\Delta}{\sqrt{\Delta^2 + z_e^2}} - \frac{k_1}{2\varepsilon_1} \right) \tilde{u}^2 - \left(k_1 \frac{\Delta}{\sqrt{\Delta^2 + z_e^2}} - \frac{k_1}{2\varepsilon_2} \right) \tilde{w}^2 + \frac{\varepsilon_1}{2} \dot{u}^2 + \frac{\varepsilon_2}{2} \dot{w}^2 \end{aligned} \quad (20)$$

$$\left\{ \begin{array}{l} \alpha = \arctan \left(\frac{\tilde{w}}{\tilde{u}} \right) \\ \dot{\alpha} = \frac{\alpha(t + \Delta t) - \alpha(t)}{\Delta t} \end{array} \right. \quad (15)$$

Note that Δt of the second equation in (15) can be chosen as the step size in simulation.

3.1.3. Stability analyses of the kinematics subsystem

Theorem 1. Consider the trajectory tracking error dynamics (9), suppose a desired trajectory is given that the **Assumption 1** is satisfied, then under the velocity observers (10-11), LOS guidance law (12), kinematics control law (13-15), the trajectory tracking error vectors are guaranteed to converge to a specified compact set.

Proof. Consider the following Lyapunov function candidate for kinematics control:

$$V_1 = \frac{1}{2} x_e^2 + \frac{1}{2} z_e^2 + \frac{1}{2} (v_e - v_{LOS})^2 + \frac{1}{2} \tilde{u}^2 + \frac{1}{2} \tilde{w}^2 \quad (16)$$

where $\tilde{u} = \hat{u} - u$, $\tilde{w} = \hat{w} - w$.

Differentiating (16) yields

$$\begin{aligned} \dot{V}_1 &= x_e \dot{x}_e + z_e \dot{z}_e + (v_e - v_{LOS}) (\dot{v}_e - \dot{v}_{LOS}) + \tilde{u} \dot{\tilde{u}} + \tilde{w} \dot{\tilde{w}} \\ &= x_e \left[u \frac{\cos v_e}{\cos \alpha} - U_d (1 + \kappa z_e) \right] + z_e \left[-u \frac{\sin v_e}{\cos \alpha} + \kappa U_d x_e \right] \\ &+ (v_e - v_{LOS}) \left(q - \dot{\alpha} - \dot{v}_d - \dot{v}_{LOS} \right) + \tilde{u} (\hat{u} - \dot{u}) + \tilde{w} (\hat{w} - \dot{w}) \\ &= x_e u \frac{\cos v_e}{\cos \alpha} - x_e U_d - z_e u \frac{\sin v_e}{\cos \alpha} + (v_e - v_{LOS}) \left(q - \dot{\alpha} - \dot{v}_d - \dot{v}_{LOS} \right) \\ &+ \tilde{u} (\hat{u} - \dot{u}) + \tilde{w} (\hat{w} - \dot{w}) \end{aligned} \quad (17)$$

Based on (9–11), one can obtain:

$$\dot{\hat{u}} = \dot{p}_u + k_1 \dot{x}_e = k_1 [-\tilde{u} \cos(\theta - v_d) - \tilde{w} \sin(\theta - v_d)] \quad (18)$$

$$\dot{\hat{w}} = \dot{p}_w + k_1 \dot{z}_e = k_1 [\tilde{u} \sin(\theta - v_d) - \tilde{w} \cos(\theta - v_d)] \quad (19)$$

Substituting (12–13) and (18–19) into (17), one can obtain:

where $\varepsilon_1 > 0$, $\varepsilon_2 > 0$.

According to (14), the further derivations of (20) can be divided into following two cases:

(1) When $v_e - v_{LOS} \neq 0$, one can obtain:

$$\begin{aligned} \dot{V}_1 &\leq -k_2 x_e^2 - k_3(v_e - v_{LOS})^2 - k_1 \left(\frac{\Delta}{\sqrt{\Delta^2 + z_e^2}} - \frac{1}{2\varepsilon_1} \right) \tilde{u}^2 \\ &- k_1 \left(\frac{\Delta}{\sqrt{\Delta^2 + z_e^2}} - \frac{1}{2\varepsilon_2} \right) \tilde{w}^2 + \frac{\varepsilon_1}{2} \dot{u}^2 + \frac{\varepsilon_2}{2} \dot{w}^2 \end{aligned} \quad (21)$$

(2) When $v_e - v_{LOS} = 0$, (20) can be further derived as:

$$\begin{aligned} \dot{V}_1 &\leq -k_2 x_e^2 - U \frac{z_e^2}{\sqrt{\Delta^2 + z_e^2}} - k_1 \left(\frac{\Delta}{\sqrt{\Delta^2 + z_e^2}} - \frac{1}{2\varepsilon_1} \right) \tilde{u}^2 \\ &- k_1 \left(\frac{\Delta}{\sqrt{\Delta^2 + z_e^2}} - \frac{1}{2\varepsilon_2} \right) \tilde{w}^2 + \frac{\varepsilon_1}{2} \dot{u}^2 + \frac{\varepsilon_2}{2} \dot{w}^2 \end{aligned} \quad (22)$$

Since it is always possible to choose the parameters ε_1 and ε_2 to

guarantee $\frac{A}{\sqrt{\Delta^2 + z_e^2}} - \frac{1}{2\varepsilon_1} \geq 0$ and $\frac{A}{\sqrt{\Delta^2 + z_e^2}} - \frac{1}{2\varepsilon_2} \geq 0$, and considering the fact that \dot{u} and \dot{w} are bounded (**Remark 2**), it can be concluded from (21) and (22) that under the velocity observers (10–11), LOS guidance law (12), kinematics control law (13–15), the trajectory tracking error vectors are guaranteed to converge to a specified compact set.

3.2. Dynamics controller design

3.2.1. Disturbance observer design

Since the velocities u and w are unmeasurable, utilizing the velocity observers (10–11), the dynamics model (3) is rewritten as

$$\begin{cases} \dot{\hat{u}} = f_u(\hat{u}, \hat{w}, q) + g_u X_T + d_u \\ \dot{\hat{w}} = f_w(\hat{u}, \hat{w}, q) + g_w \tau_w + d_w \\ \dot{q} = f_q(\hat{u}, \hat{w}, q) + g_q \tau_q + d_q \end{cases} \quad (23)$$

To estimate the unknown compound environmental disturbances, following disturbance observers are designed:

$$\begin{cases} \dot{\hat{d}_u} = m_u + k_4 \hat{u} \\ \dot{m}_u = -k_4 (f_u(\hat{u}, \hat{w}, q) + g_u X_T + \hat{d}_u) \end{cases} \quad (24)$$

$$\begin{cases} \dot{\hat{d}_w} = m_w + k_5 \hat{w} \\ \dot{m}_w = -k_5 (f_w(\hat{u}, \hat{w}, q) + g_w \tau_w + \hat{d}_w) \end{cases} \quad (25)$$

$$\begin{cases} \dot{\hat{d}_q} = m_q + k_6 q \\ \dot{m}_q = -k_6 (f_q(\hat{u}, \hat{w}, q) + g_q \tau_q + \hat{d}_q) \end{cases} \quad (26)$$

where m_u , m_w , and m_q are the designed auxiliary variables, k_4 , k_5 , and k_6 are positive observer gains.

Note that compared with conventional disturbance observer method, the proposed method utilizes the estimated velocities rather than the measured values.

3.2.2. Surge velocity tracking controller design

In this subsection, the control input X_T is derived, so that the surge velocity \hat{u} can converge to the desired surge velocity u_d as t goes to ∞ .

Define the surge velocity tracking error as

$$z_u = \hat{u} - u_d \quad (27)$$

In order to achieve surge velocity tracking, sliding mode control method will be utilized, and a modified integral sliding mode surface is chosen as:

$$s_u = z_u + c_u \int_0^t \tanh(z_u) dt - s_u(0) e^{-\lambda_u t} \quad (28)$$

where $c_u > 0$, $\lambda_u > 0$, $s_u(0)$ represents the initial value of the sliding mode surface. Note that compared with conventional integral sliding mode surface, $s_u(0)e^{-\lambda_u t}$ is considered in the proposed sliding mode surface, which helps avoiding excessive initial deviation. Besides, the $\tanh(\cdot)$ function is utilized to help avoiding “Integral explosion” problem caused by excessive surge velocity tracking error.

Differentiating (28) yields

$$\begin{aligned} \dot{s}_u &= \dot{z}_u + c_u \tanh(z_u) + \lambda_u s_u(0) e^{-\lambda_u t} \\ &= f_u(\hat{u}, \hat{w}, q) + g_u X_T + d_u - \dot{u}_d + c_u \tanh(z_u) + \lambda_u s_u(0) e^{-\lambda_u t} \end{aligned} \quad (29)$$

To improve the convergence efficiency and force the system states toward the given sliding manifold, following modified terminal approaching law is employed:

$$\dot{s}_u = -\mu_u s_u - \sigma_u |s_u|^{r_u} \tanh(s_u) \quad (30)$$

where $\mu_u > 0$, $\sigma_u > 0$, $0 < r_u < 1$. Note that the $\tanh(\cdot)$ function is utilized to replace the $\text{sign}(\cdot)$ function to weaken the chattering problem.

Based on (29) and (30), the control input X_T is designed as:

$$\begin{aligned} X_T = &\frac{1}{g_u} [-\mu_u s_u - \sigma_u |s_u|^{r_u} \tanh(s_u) - f_u(\hat{u}, \hat{w}, q) \\ &+ \dot{u}_d - c_u \tanh(z_u) - \lambda_u s_u(0) e^{-\lambda_u t} - \hat{d}_u] \end{aligned} \quad (31)$$

However, considering the actuator saturation problem, the actual control input will be $\text{sat}(X_T)$, where $\text{sat}(\cdot)$ denotes the nonlinear saturation characteristic, which can be written as:

$$\text{sat}(X_T) = \begin{cases} \bar{X}_T & X_T > \bar{X}_T \\ X_T & |X_T| \leq \bar{X}_T \\ -\bar{X}_T & X_T < -\bar{X}_T \end{cases} \quad (32)$$

To solve the problem of actuator saturation, following anti-windup compensator is employed (Cui et al., 2016):

$$\dot{\zeta} = \begin{cases} -k\zeta - \frac{|g_u s_u \Delta X_T| + \frac{1}{2} (\Delta X_T)^2}{|\zeta|^2} \zeta + \Delta X_T, & |\zeta| \geq \vartheta \\ 0, & |\zeta| < \vartheta \end{cases} \quad (33)$$

where $\Delta X_T = \text{sat}(X_T) - X_T$, ζ is the designed auxiliary state, $k > 0$ is a designed parameter, and ϑ is a small positive constant.

3.2.3. Pitch angular velocity tracking controller design

In this subsection, the control inputs δ_1 , δ_2 , δ_3 , δ_4 will be derived, so that the pitch angular velocity q can converge to the desired pitch angular velocity q_d as t goes to ∞ . The pitch angular velocity tracking controller will be derived in following two steps:

Step 1: Calculation of desired rudder torque τ_{qd} .

Define the pitch angular velocity tracking error as

$$z_q = q - q_d \quad (34)$$

Similar with surge velocity tracking, terminal sliding mode control method is utilized, and the sliding mode surface is chosen as:

$$s_q = z_q + c_q \int_0^t \tanh(z_q) dt - s_q(0) e^{-\lambda_q t} \quad (35)$$

where $c_q > 0$, $\lambda_q > 0$.

Differentiating (35) yields

$$\begin{aligned} \dot{s}_q &= \dot{z}_q + c_q \tanh(z_q) + \lambda_q s_q(0) e^{-\lambda_q t} \\ &= f_q(\hat{u}, \hat{w}, q) + g_q \tau_q + d_q - \dot{q}_d + c_q \tanh(z_q) + \lambda_q s_q(0) e^{-\lambda_q t} \end{aligned} \quad (36)$$

To obtain desired rudder torque τ_{qd} , following terminal approaching law is employed:

$$\dot{s}_q = -\mu_q s_q - \sigma_q |s_q|^{r_q} \tanh(s_q) \quad (37)$$

Based on (36) and (37), the desired rudder torque τ_{qd} is derived as:

$$\begin{aligned} \tau_{qd} = &\frac{1}{g_q} [-\mu_q s_q - \sigma_q |s_q|^{r_q} \tanh(s_q) - f_q(\hat{u}, \hat{w}, q) + \dot{q}_d - c_q \tanh(z_q) \\ &- \lambda_q s_q(0) e^{-\lambda_q t} - \hat{d}_q] \end{aligned} \quad (38)$$

Step 2: Calculation of control inputs δ_1 , δ_2 , δ_3 , δ_4 .

Solving the rudder angles from the rudder torque is a SIMO problem, the solution is not unique. To obtain the optimal solution, a multi-objective optimization method is utilized for rudder angle calculation. The performance index for the optimal rudder angle calculation block is constructed with following two objectives:

- (1) Minimum rudder torque error: The actual rudder torque generated by the four rudder angles can approximate the desired torque in (38) with minimum error;
- (2) Minimum control effect: The control effect of the rudders is the smallest.

The cost function J is defined as:

Table 1
Parameters of X-rudder AUV model.

$m = 30.48 \text{ kg}$	$Z_{w w} = -131 \text{ kg/m}$	$M_{uq} = -2 \text{ kg}\cdot\text{m/rad}$
$W = 299 \text{ N}$	$Z_{q q} = -0.632 \text{ kg}\cdot\text{m/rad}^2$	$M_{uw} = 24 \text{ kg}$
$B = 306 \text{ N}$	$Z_{uq} = -5.22 \text{ kg/rad}$	$M_{\dot{q}} = -4.88 \text{ kg}\cdot\text{m}^2/\text{rad}$
$x_g = 0$	$Z_{uw} = -28.6 \text{ kg/m}$	$I_{yy} = 3.45 \text{ kg}\cdot\text{m}^2$
$z_g = 0.0196 \text{ m}$	$Z_{\dot{w}} = -35.5 \text{ kg}$	$M_{uu\delta_1} = -2.1744 \text{ kg/rad}$
$x_b = -0.611 \text{ m}$	$Z_{uu\delta_1} = -3.4083 \text{ kg}/(\text{m}\cdot\text{rad})$	$M_{uu\delta_2} = 2.1744 \text{ kg/rad}$
$z_b = 0$	$Z_{uu\delta_2} = 3.4083 \text{ kg}/(\text{m}\cdot\text{rad})$	$M_{uu\delta_3} = -2.1744 \text{ kg/rad}$
$X_{u u} = -1.62 \text{ kg/m}$	$Z_{uu\delta_3} = -3.4083 \text{ kg}/(\text{m}\cdot\text{rad})$	$M_{uu\delta_4} = 2.1744 \text{ kg/rad}$
$X_u = -0.93 \text{ kg}$	$Z_{uu\delta_4} = 3.4083 \text{ kg}/(\text{m}\cdot\text{rad})$	$\bar{X}_T = 6.48 \text{ N}$
$X_{wq} = -35.5 \text{ kg/rad}$	$M_{w w} = 3.18 \text{ kg}$	$\bar{\delta} = 30^\circ$
$X_{qq} = -1.93 \text{ kg/m/rad}$	$M_{q q} = -188 \text{ kg}\cdot\text{m}^2/\text{rad}^2$	

$$\left\{ \begin{array}{l} \min J = \underbrace{\xi(\tau_q - \tau_{qd})^2}_{\text{Rudder torque allocation error}} + \underbrace{(1-\xi)\delta^T\delta}_{\text{Control effect}} \\ \text{s.t. } 0 \leq \xi \leq 1 \\ \tau_q = M_{uu\delta_1}u^2\delta_1 + M_{uu\delta_2}u^2\delta_2 + M_{uu\delta_3}u^2\delta_3 + M_{uu\delta_4}u^2\delta_4 \\ \delta = [\delta_1, \delta_2, \delta_3, \delta_4]^T \\ |\delta| \leq \bar{\delta} \end{array} \right. \quad (39)$$

where ξ is the weight coefficient utilized to balance the two optimization objectives. Besides, the limitations of rudder angle are considered during the multi-objective optimization.

Note that the selection of parameter ξ will affect the optimization objective, for instance, a larger ξ means more concentration on trajectory tracking performance, whereas a smaller ξ means more attention is paid to energy consumption. Generally, when the devices of the underwater vehicle are all normal, the energy consumption problem will be considered, but when sensor or actuator failures occur, the trajectory tracking mission will be a priority, and the energy consumption problem will be less considered or even ignored. The effect of parameter ξ on the control performance will be verified in section 4.

Moreover, sequential quadratic programming (SQP) algorithm is applied in this paper to solve the multi-objective optimization problem. SQP is an effective method for constraint optimization problem, which is implemented in following three subsections: (1) Updating of the Hessian

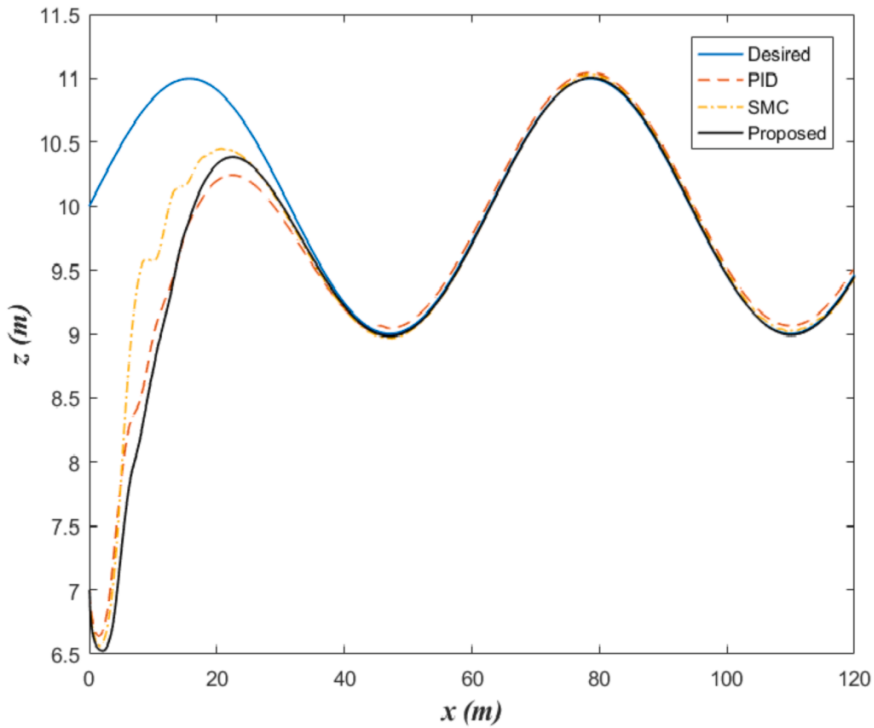


Fig. 4. Trajectory tracking comparison.

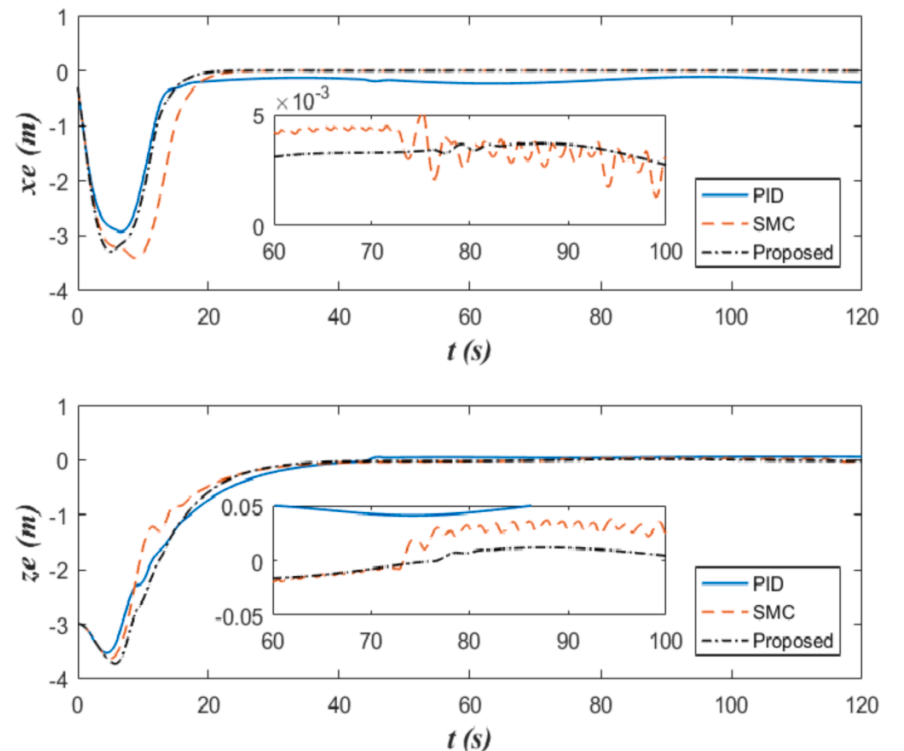


Fig. 5. Tracking error comparison.

matrix of the Lagrangian function; (2) Quadratic programming problem solution; (3) Line search and merit function calculation.

Domain iterative calculation process of SQP is presented as follows:

- (1) Choose initial state of optimization variable δ_0 and Hessian matrix H_0 ;
- (2) Solve QP sub problem, get search direction d_k ;
- (3) Update optimization variable δ_k and Hessian matrix H_k based on search direction d_k ;
- (4) Calculate the objective function in the form of Lagrangian function L_k ;
- (5) Determine whether the objective function J_k is convergent, if yes, jump to step (6); otherwise, repeat step (2–5);
- (6) End iteration.

Remark 3. The proposed optimal rudder angle calculation method is not only energy efficient but also robust against rudder failures, helps tackle the rudder torque error convergence problem and input

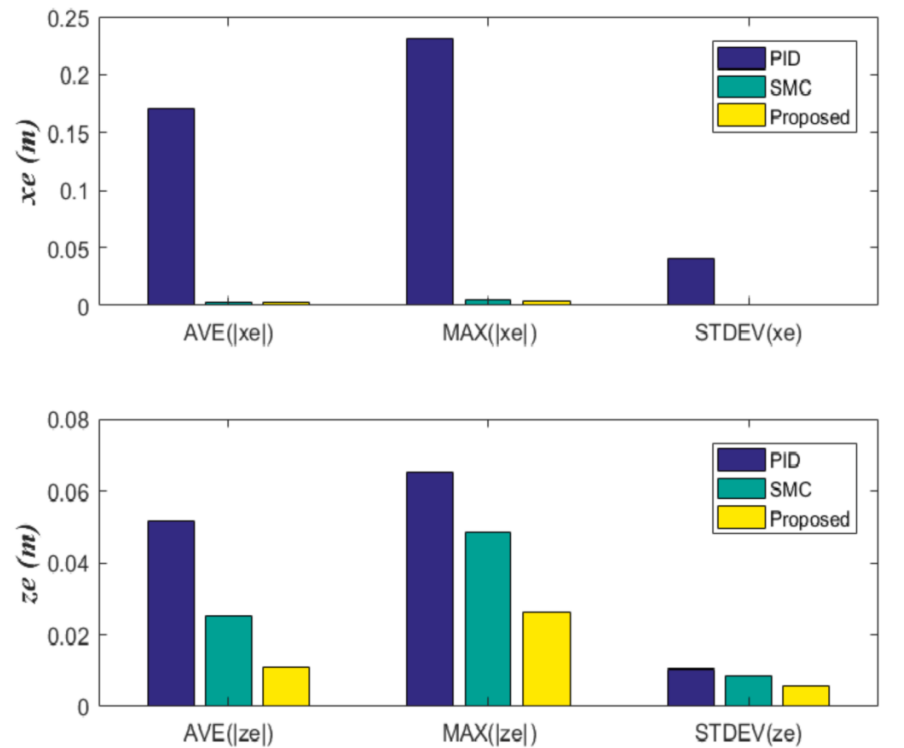


Fig. 6. Data analysis of steady-state tracking errors.

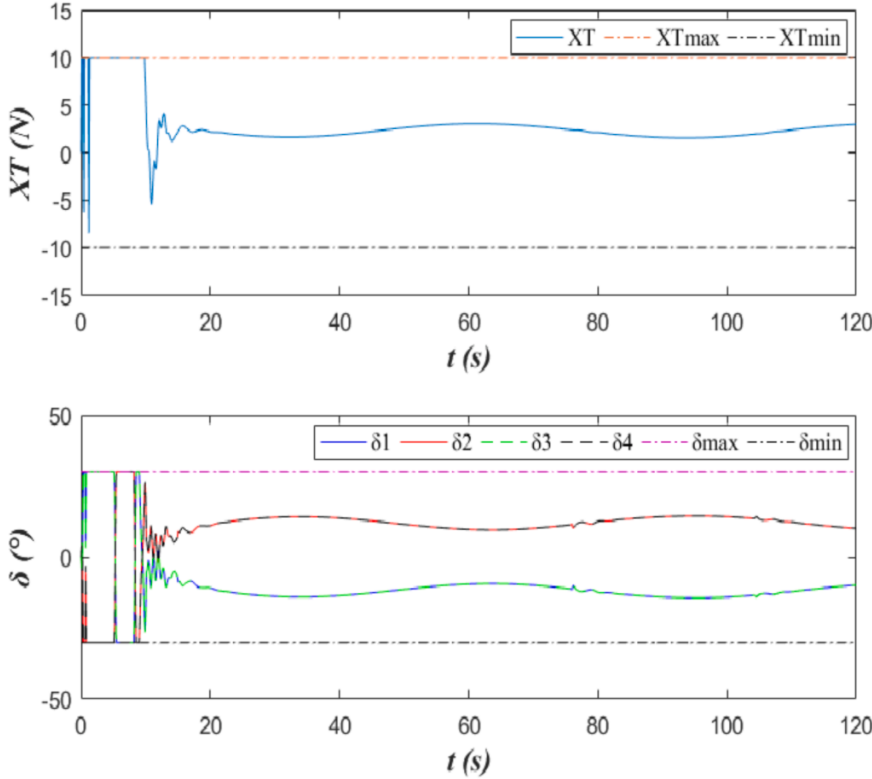


Fig. 7. Control inputs of proposed method.

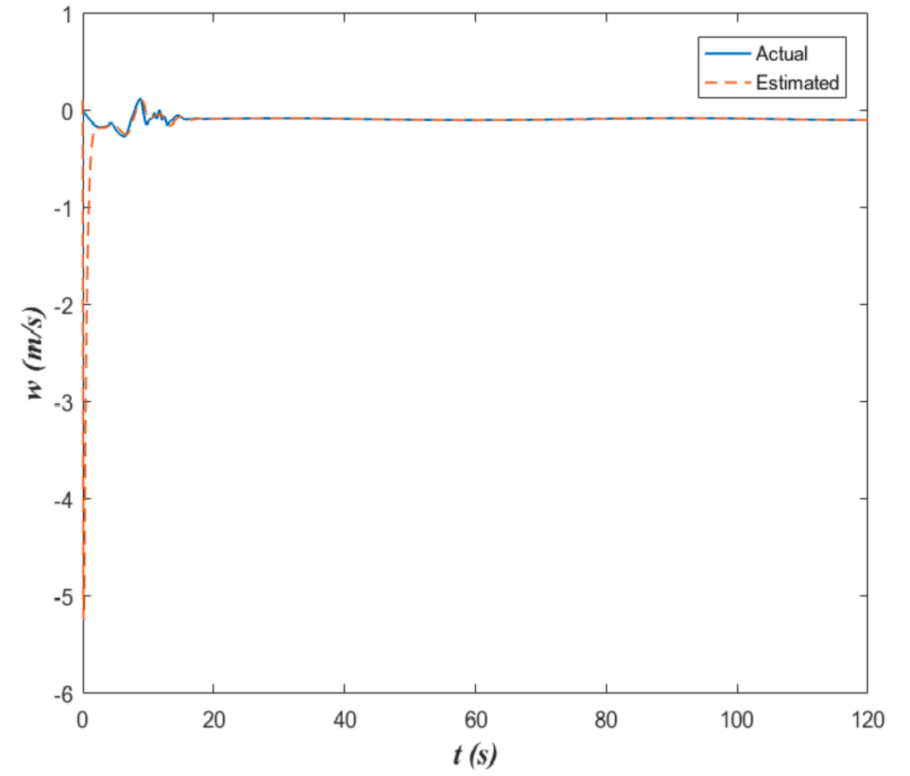
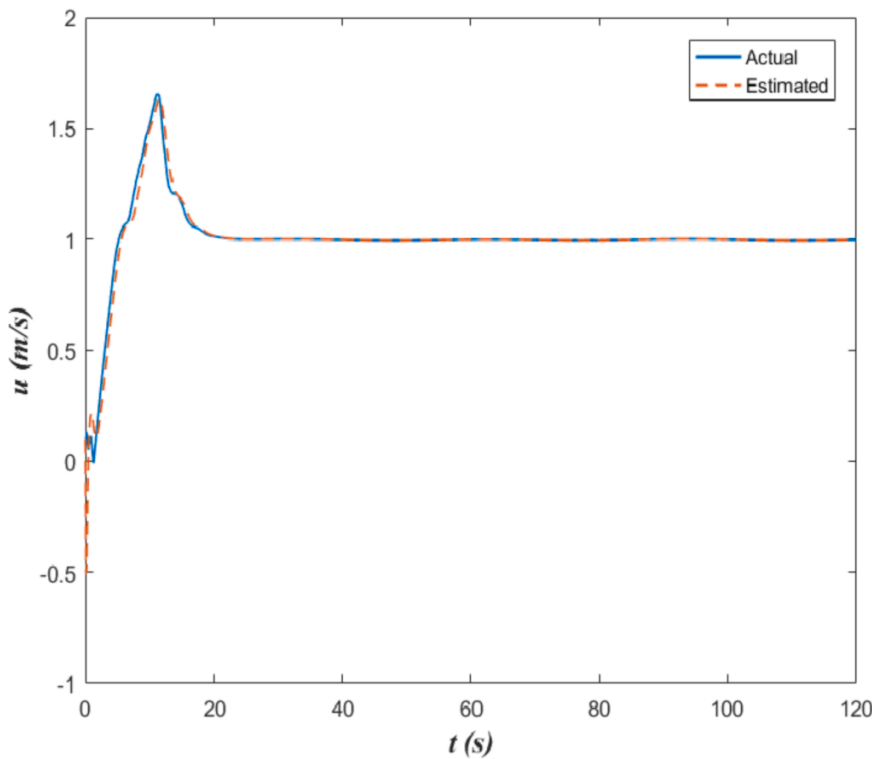
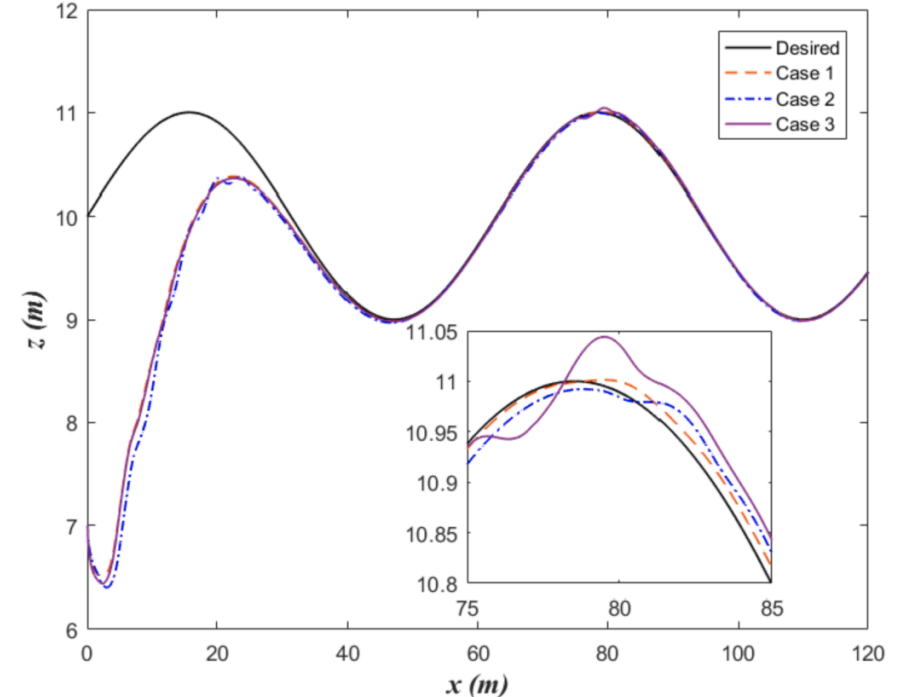
Fig. 9. Estimate of heave velocity w .Fig. 8. Estimate of surge velocity u .

Fig. 10. Trajectories under different disturbances.

saturation problem.

3.2.4. Stability analyses of the dynamics subsystem

Theorem 2. Consider the dynamics model (23), the desired surge velocity u_d and desired pitch angular velocity q_d derived in (13-15), utilizing the disturbance observers (24-26), propeller input (31-33), and rudder input (38-39), the surge velocity tracking error (27) and pitch angular velocity tracking error (34) are guaranteed to converge to a specified compact set.

Proof. Consider the following Lyapunov function candidate for dynamics control:

$$V_2 = \frac{1}{2}s_u^2 + \frac{1}{2}s_q^2 + \frac{1}{2}\tilde{d}_u^2 + \frac{1}{2}\tilde{d}_q^2 + \frac{1}{2}\tilde{u}^2 + \frac{1}{2}\tilde{w}^2 + \frac{1}{2}\zeta^2 \quad (40)$$

where $\tilde{d}_u = \hat{d}_u - d_u$, $\tilde{d}_q = \hat{d}_q - d_q$, $\tilde{u} = \hat{u} - u$, $\tilde{w} = \hat{w} - w$.

Differentiating (40) yields:

$$\dot{V}_2 = s_u \dot{s}_u + s_q \dot{s}_q + \tilde{d}_u \dot{\tilde{d}}_u + \tilde{d}_q \dot{\tilde{d}}_q + \tilde{u} \dot{\tilde{u}} + \tilde{w} \dot{\tilde{w}} + \zeta \dot{\zeta} = s_u \dot{s}_u + s_q \dot{s}_q + \tilde{d}_u \left(\dot{\hat{d}}_u - \dot{d}_u \right) + \tilde{d}_q \left(\dot{\hat{d}}_q - \dot{d}_q \right) + \tilde{u} (\dot{\hat{u}} - \dot{u}) + \tilde{w} (\dot{\hat{w}} - \dot{w}) + \zeta \dot{\zeta} \quad (41)$$

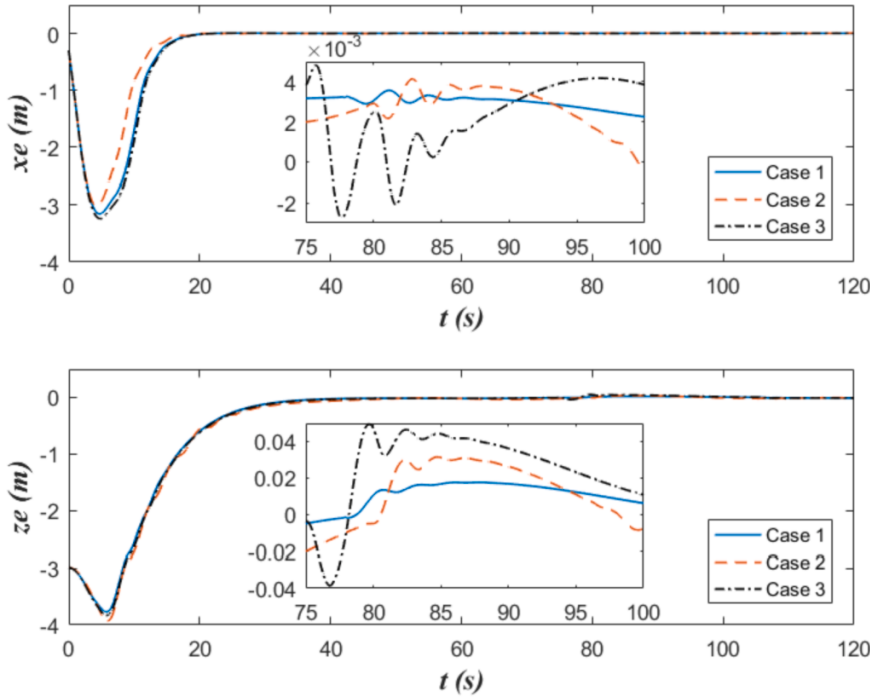


Fig. 11. Tracking errors under different disturbances.

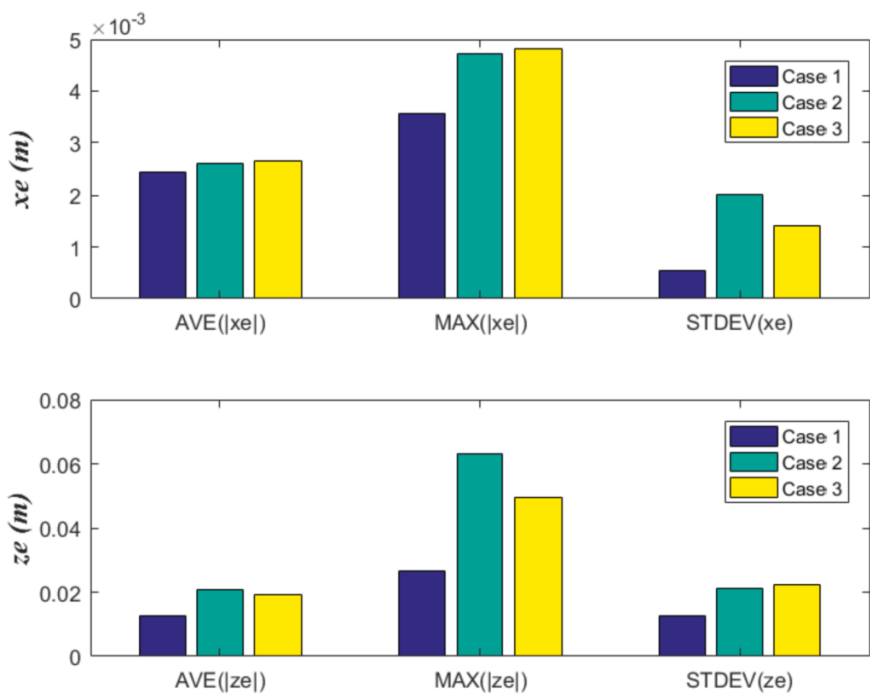
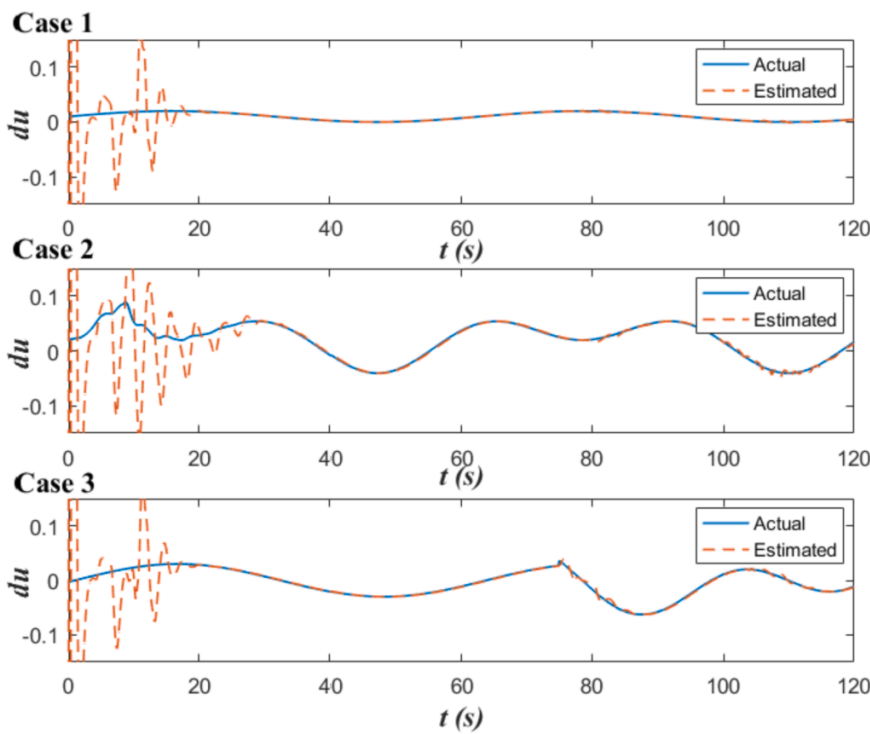
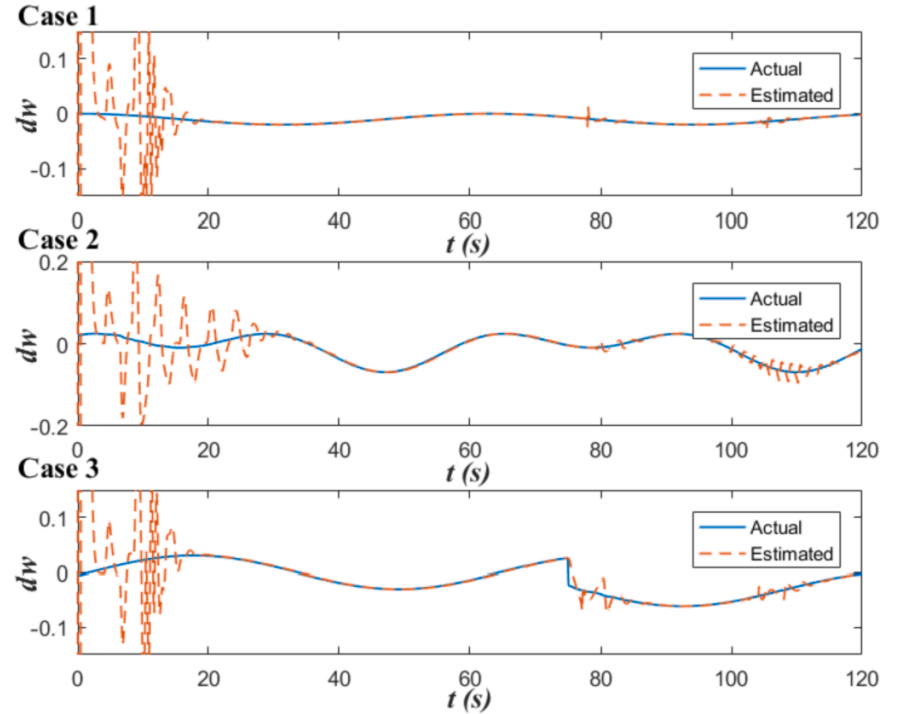
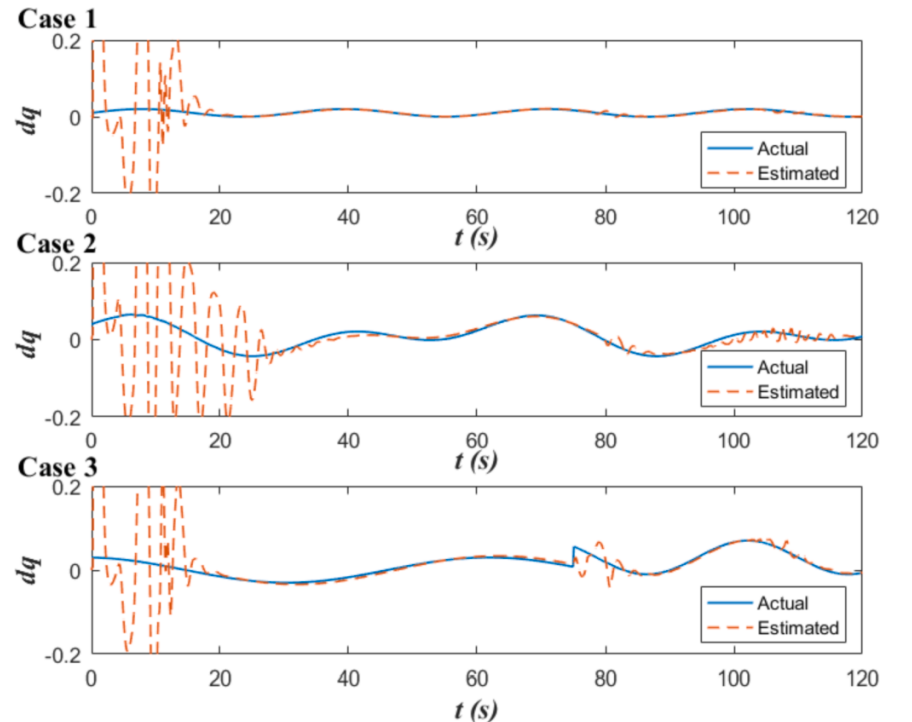


Fig. 12. Data analysis of steady-state tracking errors.

Fig. 13. Estimate of d_u in different cases.Fig. 14. Estimate of d_w in different cases.Fig. 15. Estimate of d_q in different cases.

Based on (29–33) and (36–39), one can obtain:

$$\begin{cases} \dot{s}_u = -\mu_u s_u - \sigma_u |s_u|^{r_u} \tanh(s_u) - \tilde{d}_u + g_u \Delta X_T + g_u \zeta \\ \dot{s}_q = -\mu_q s_q - \sigma_q |s_q|^{r_q} \tanh(s_q) - \tilde{d}_q + g_q (\tau_q - \tau_{qd}) \end{cases} \quad (42)$$

Based on (23), (24), and (26), one can obtain:

Table 2
Rudder stuck settings.

Case no.	Stuck Rudder no.	Stuck angle
4	Rudder 1	0°
5	Rudder 1	10°
6	Rudder 1	20°
7	Rudder 1	30°
8	Rudder 1, Rudder 2	0°, 0°

$$\left\{ \begin{array}{l} \dot{\tilde{d}}_u = -k_4 \tilde{d}_u \dot{\tilde{d}}_q = -k_6 \tilde{d}_q \end{array} \right. \quad (43)$$

Substituting (18–19), (33), and (42–43) into (41) yields:

$$\begin{aligned} \dot{V}_2 &= s_u [-\mu_u s_u - \sigma_u |s_u|^{r_u} \tanh(s_u) - \tilde{d}_u + g_u \Delta X_T + g_u \zeta] + s_q [-\mu_q s_q - \sigma_q |s_q|^{r_q} \tanh(s_q) - \tilde{d}_q + g_q (\tau_q - \tau_{qd})] \\ &\quad + \tilde{d}_u (-k_4 \tilde{d}_u - \dot{d}_u) + \tilde{d}_q (-k_6 \tilde{d}_q - \dot{d}_q) - \left(k_1 \frac{\Delta}{\sqrt{\Delta^2 + z_e^2}} - \frac{k_1}{2\varepsilon_1} \right) \tilde{u}^2 - \left(k_1 \frac{\Delta}{\sqrt{\Delta^2 + z_e^2}} - \frac{k_1}{2\varepsilon_2} \right) \tilde{w}^2 + \frac{\varepsilon_1}{2} \dot{u}^2 + \frac{\varepsilon_2}{2} \dot{w}^2 \\ &\quad + \zeta \left[-k\zeta - \frac{|g_u s_u \Delta X_T| + \frac{1}{2} (\Delta X_T)^2}{|\zeta|^2} \zeta + \Delta X_T \right] \\ &= -\mu_u s_u^2 - \sigma_u |s_u|^{r_u} s_u \tanh(s_u) - s_u \tilde{d}_u + s_u g_u \Delta X_T + s_u g_u \zeta - \mu_q s_q^2 - \sigma_q |s_q|^{r_q} s_q \tanh(s_q) - s_q \tilde{d}_q + s_q g_q (\tau_q - \tau_{qd}) \\ &\quad - k_4 \tilde{d}_u^2 - \tilde{d}_u \dot{d}_u - k_6 \tilde{d}_q^2 - \tilde{d}_q \dot{d}_q - \left(k_1 \frac{\Delta}{\sqrt{\Delta^2 + z_e^2}} - \frac{k_1}{2\varepsilon_1} \right) \tilde{u}^2 - \left(k_1 \frac{\Delta}{\sqrt{\Delta^2 + z_e^2}} - \frac{k_1}{2\varepsilon_2} \right) \tilde{w}^2 + \frac{\varepsilon_1}{2} \dot{u}^2 + \frac{\varepsilon_2}{2} \dot{w}^2 \\ &\quad - k\zeta^2 - |g_u s_u \Delta X_T| - \frac{1}{2} (\Delta X_T)^2 + \zeta \Delta X_T \\ &\leq -\mu_u s_u^2 - \sigma_u |s_u|^{r_u} s_u \tanh(s_u) + |s_u \tilde{d}_u| + |s_u g_u \zeta| - \mu_q s_q^2 - \sigma_q |s_q|^{r_q} s_q \tanh(s_q) + |\tilde{d}_q| + |s_q g_q (\tau_q - \tau_{qd})| \\ &\quad - k_4 \tilde{d}_u^2 + |\tilde{d}_u \dot{d}_u| - k_6 \tilde{d}_q^2 + |\tilde{d}_q \dot{d}_q| - \left(k_1 \frac{\Delta}{\sqrt{\Delta^2 + z_e^2}} - \frac{k_1}{2\varepsilon_1} \right) \tilde{u}^2 - \left(k_1 \frac{\Delta}{\sqrt{\Delta^2 + z_e^2}} - \frac{k_1}{2\varepsilon_2} \right) \tilde{w}^2 + \frac{\varepsilon_1}{2} \dot{u}^2 + \frac{\varepsilon_2}{2} \dot{w}^2 \\ &\quad - k\zeta^2 - \frac{1}{2} (\Delta X_T)^2 + |\zeta \Delta X_T| \end{aligned} \quad (44)$$

Since there exists:

$$\left\{ \begin{array}{l} |s_u \tilde{d}_u| \leq \frac{1}{2\varepsilon_3} s_u^2 + \frac{\varepsilon_3}{2} \tilde{d}_u^2 \\ |s_q \tilde{d}_q| \leq \frac{1}{2\varepsilon_4} s_q^2 + \frac{\varepsilon_4}{2} \tilde{d}_q^2 \\ |\tilde{d}_u \dot{d}_u| \leq \frac{1}{2\varepsilon_5} \tilde{d}_u^2 + \frac{\varepsilon_5}{2} \dot{d}_u^2 \\ |\tilde{d}_q \dot{d}_q| \leq \frac{1}{2\varepsilon_6} \tilde{d}_q^2 + \frac{\varepsilon_6}{2} \dot{d}_q^2 \\ |s_u g_u \zeta| \leq \frac{g_u^2}{2\varepsilon_7} s_u^2 + \frac{\varepsilon_7}{2} \zeta^2 \\ |s_q g_q (\tau_q - \tau_{qd})| \leq \frac{g_q^2}{2\varepsilon_8} s_q^2 + \frac{\varepsilon_8}{2} (\tau_q - \tau_{qd})^2 \\ |\zeta \Delta X_T| \leq \frac{1}{2\varepsilon_9} \zeta^2 + \frac{\varepsilon_9}{2} (\Delta X_T)^2 \end{array} \right. \quad (45)$$

where $\varepsilon_3 > 0$, $\varepsilon_4 > 0$, $\varepsilon_5 > 0$, $\varepsilon_6 > 0$, $\varepsilon_7 > 0$, $\varepsilon_8 > 0$, $\varepsilon_9 > 0$.

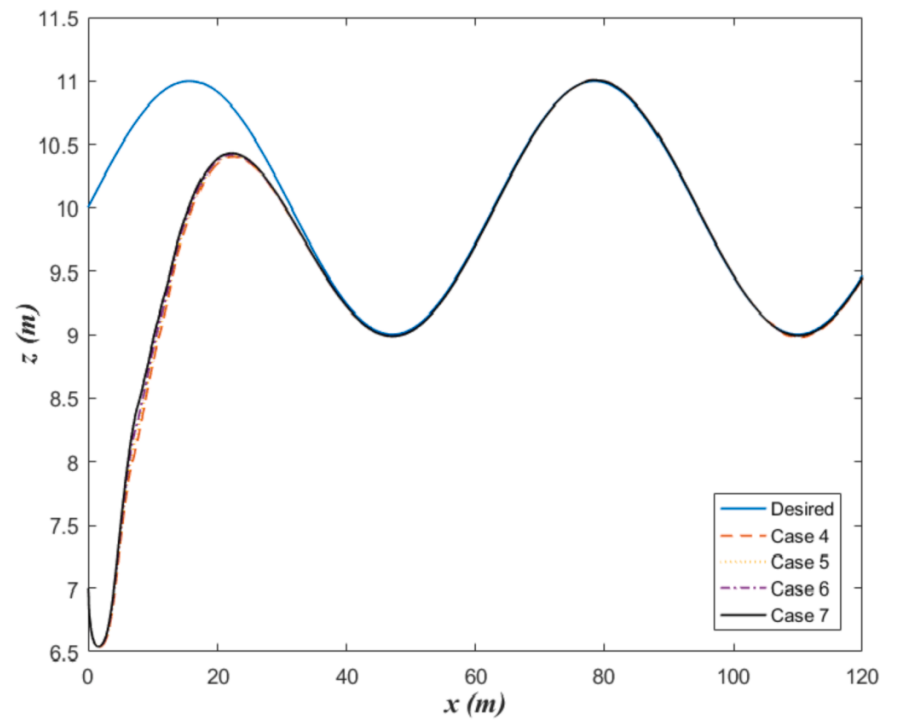


Fig. 16. Trajectories with one rudder stuck ($\xi = 0.5$).

The time-derivative of V_2 can be further derived as:

$$\begin{aligned} \dot{V}_2 \leq & -\left(\mu_u - \frac{1}{2\varepsilon_3} - \frac{g_u^2}{2\varepsilon_7}\right)s_u^2 - \sigma_u|s_u|^{r_u}s_u \tanh(s_u) - \left(\mu_q - \frac{1}{2\varepsilon_4} - \frac{g_q^2}{2\varepsilon_8}\right)s_q^2 - \sigma_q|s_q|^{r_q}s_q \tanh(s_q) \\ & -\left(k_4 - \frac{\varepsilon_3}{2} - \frac{1}{2\varepsilon_5}\right)\tilde{d}_u^2 - \left(k_6 - \frac{\varepsilon_4}{2} - \frac{1}{2\varepsilon_6}\right)\tilde{d}_q^2 - \left(k_1 \frac{\Delta}{\sqrt{\Delta^2 + z_e^2}} - \frac{k_1}{2\varepsilon_1}\right)\tilde{u}^2 \\ & -\left(k_1 \frac{\Delta}{\sqrt{\Delta^2 + z_e^2}} - \frac{k_1}{2\varepsilon_2}\right)\tilde{w}^2 - \left(k - \frac{\varepsilon_7}{2} - \frac{1}{2\varepsilon_9}\right)\zeta^2 - \frac{1-\varepsilon_9}{2}(\Delta X_T)^2 \\ & +\frac{\varepsilon_1}{2}\dot{u}^2 + \frac{\varepsilon_2}{2}\dot{w}^2 + \frac{\varepsilon_5}{2}\dot{d}_u^2 + \frac{\varepsilon_6}{2}\dot{d}_q^2 + \frac{\varepsilon_8}{2}(\tau_q - \tau_{qd})^2 \end{aligned} \quad (46)$$

Since it is always possible to choose the parameters to guarantee $\mu_u - \frac{1}{2\varepsilon_3} - \frac{g_u^2}{2\varepsilon_7} \geq 0$, $\mu_q - \frac{1}{2\varepsilon_4} - \frac{g_q^2}{2\varepsilon_8} \geq 0$, $k_4 - \frac{\varepsilon_3}{2} - \frac{1}{2\varepsilon_5} \geq 0$, $k_6 - \frac{\varepsilon_4}{2} - \frac{1}{2\varepsilon_6} \geq 0$, $k_1 \frac{\Delta}{\sqrt{\Delta^2 + z_e^2}} - \frac{k_1}{2\varepsilon_1} \geq 0$, $k_1 \frac{\Delta}{\sqrt{\Delta^2 + z_e^2}} - \frac{k_1}{2\varepsilon_2} \geq 0$, $k - \frac{\varepsilon_7}{2} - \frac{1}{2\varepsilon_9} \geq 0$, $\frac{1-\varepsilon_9}{2} \geq 0$, considering the fact that \dot{u} , \dot{w} , \dot{d}_u , and \dot{d}_q are bounded (See **Remark 2** and **Assumption 2**), and $(\tau_q - \tau_{qd})^2$ is bounded thanks to the optimal rudder angle calculation method (see **Remark 3**), it can be concluded from (46) that the dynamics control subsystem is stable, and the surge velocity tracking error and pitch angular velocity tracking error are guaranteed to converge to a specified compact set.

Remark 4. Based on **Theorem 1** and **Theorem 2**, the convergence of the whole trajectory tracking system can be guaranteed.

4. Simulation results

In this section, comparative numerical simulations are carried out to verify the effectiveness and robustness of proposed control method. The simulation parameters are introduced in [subsection 4.1](#), and the simulation results are presented in [subsections 4.2-4.4](#).

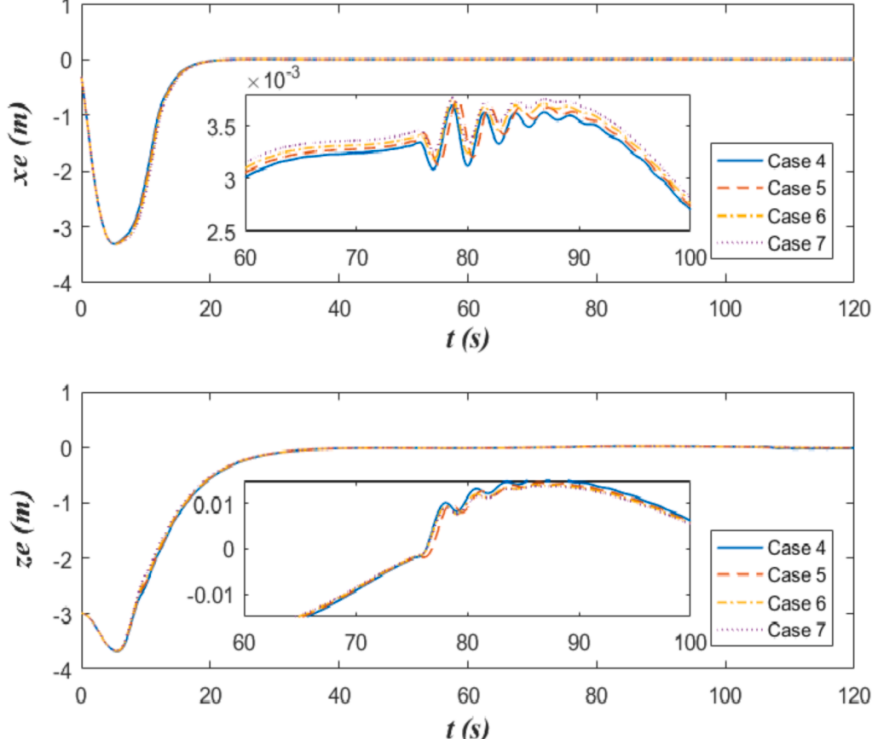


Fig. 17. Tracking error with one rudder stuck ($\xi = 0.5$).

4.1. Parameter selection

Numerical simulations are carried out with a x-rudder AUV, and the parameters of AUV model are given in [Table 1](#).

The parameters of the proposed controller are designed as follows: the gain of linear velocity observer is selected as $k_1 = 1.75$, the look-ahead distance is $\Delta = 2.772$, the gains of kinematics controller are selected as $k_2 = 0.5$, $k_3 = 2$, the gains of disturbance observers are chosen as $k_4 = k_5 = k_6 = 2.5$, the gains of surge velocity tracking controller are $c_u = 1.5$, $\lambda_u = 1$, $\mu_u = 0.0001$, $\sigma_u = 0.0001$, $r_u = 0.9$, the gains of pitch angular velocity tracking controller are $c_q = 0.15$, $\lambda_q = 0.5$, $\mu_q = 10$, $\sigma_q = 10$, $r_q = 0.9$, and the weight coefficient utilized in optimal rudder allocation is selected as $\xi = 0.5$.

For comparison purpose, the other two control methods are utilized, which employ the same kinematics control and optimal rudder allocation method as proposed controller, whereas apply conventional PID controller and SMC (sliding mode control) for dynamics control. For PID control, the parameters for surge velocity tracking are selected as $k_p = 25$, $k_i = 0.01$, $k_d = 0$, and the parameters for pitch angular velocity tracking are selected as $k_p = 250$, $k_i = 0.01$, $k_d = 0$. For SMC, the sliding mode surfaces and controllers are designed as

$$\left\{ \begin{array}{l} s_u = z_u + c_u \int_0^t z_u dt - s_u(0)e^{-\lambda_u t} \\ s_q = z_q + c_q \int_0^t z_q dt - s_q(0)e^{-\lambda_q t} \\ X_T = \frac{1}{g_u} [-\mu_u s_u - \sigma_u \text{sign}(s_u) - f_u(\hat{u}, \hat{w}, q) + \dot{u}_d - c_u z_u - \lambda_u s_u(0)e^{-\lambda_u t} - \hat{d}_u] \\ \tau_{qd} = \frac{1}{g_q} [-\mu_q s_q - \sigma_q \text{sign}(s_q) - f_q(\hat{u}, \hat{w}, q) + \dot{q}_d - c_q z_q - \lambda_q s_q(0)e^{-\lambda_q t} - \hat{d}_q] \end{array} \right.$$

And the parameters of SMC for surge velocity tracking are selected as $c_u = 1.5$, $\lambda_u = 1$, $\mu_u = 0.0001$, $\sigma_u = 0.0001$, the parameters of SMC for pitch angular velocity tracking are selected as $c_q = 0.15$, $\lambda_q = 0.5$, $\mu_q = 8$, $\sigma_q = 1$.

4.2. Trajectory tracking performance without disturbances

In this subsection, the trajectory tracking performance of proposed controller is verified through comparison with PID control and SMC. A sinusoidal curve is chosen as the desired trajectory, which is parameterized by $x_d = 1.0t$ m and $z_d = 10 + \sin(0.1t)$ m. The initial conditions are selected as $[x(0), z(0), \theta(0)] = [0\text{m}, 7\text{m}, 0\text{rad}]$ and $[u(0), w(0), q(0)] = [0.1\text{m/s}, 0\text{m/s}, 0\text{rad/s}]$.

The trajectory tracking performance and tracking errors are shown in [Fig. 4](#) and [Fig. 5](#). It is easily observed that all the three controllers can

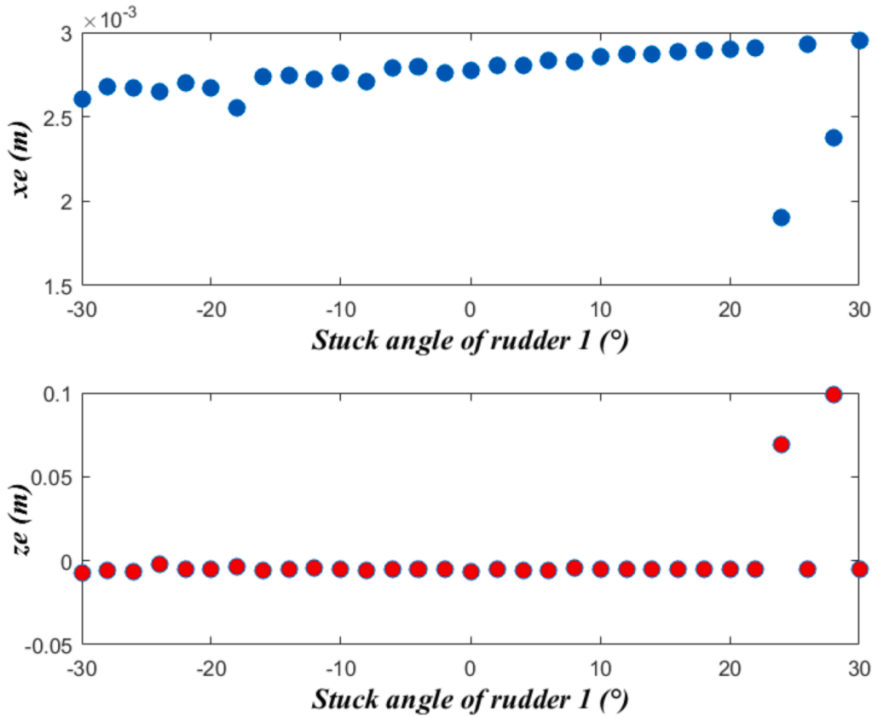


Fig. 18. Tracking errors under different rudder stuck angles ($\xi = 0.5$).

regulate the AUV to the desired trajectory, but the proposed controller shows the best transient performance. Compared with PID control, the proposed controller exhibits better tracking accuracy, while compared with SMC, the proposed controller exhibits higher stability without chattering. To further distinguish tracking performance of the three controllers, data analyses of steady-state tracking errors are shown in Fig. 6, where AVE(.) represents the average value, MAX(.) represents the maximum value, and STDEV(.) denotes the standard deviation value. It is clearly seen that proposed controller has the smallest tracking error in steady-state.

The control inputs of proposed controller are demonstrated in Fig. 7, which indicates that the proposed method can limit the control inputs into a valid range. The estimations of linear velocities are presented in Fig. 8 and Fig. 9. It is seen that the unmeasured linear velocities u and w can be well estimated by the proposed velocity observers with small estimation errors.

According to the above analyses, the proposed control scheme is proved to be effective for sinusoidal trajectory tracking, and has better transient performance than PID control and SMC method.

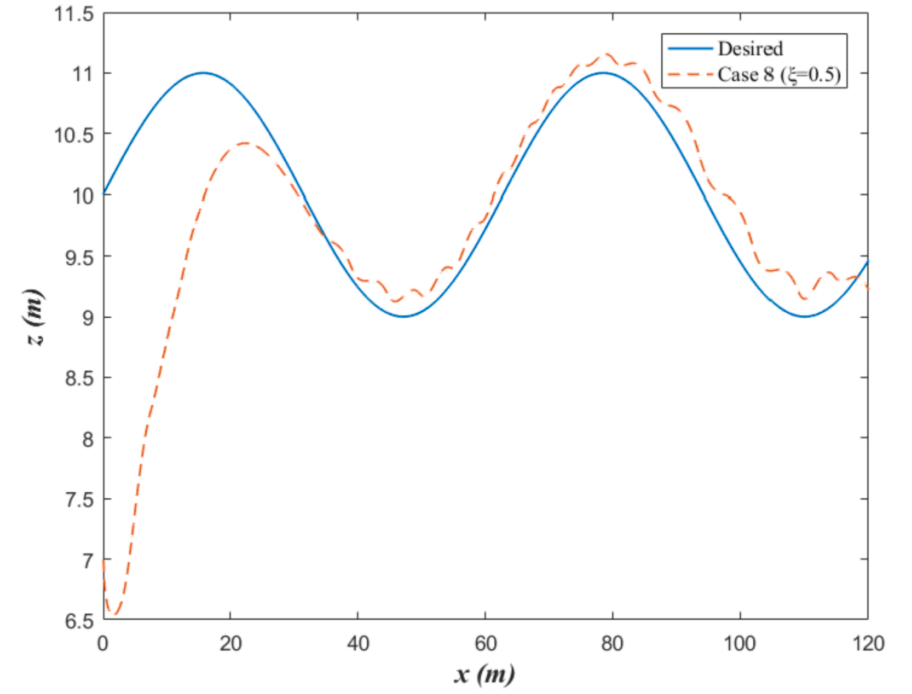


Fig. 20. Trajectory with two rudders stuck ($\xi = 0.5$).

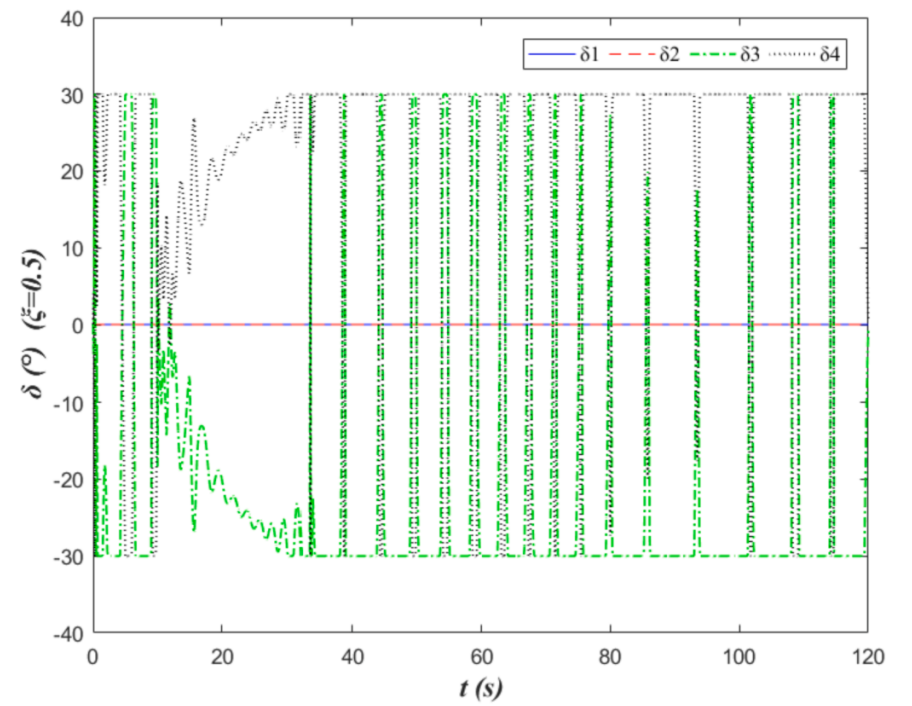


Fig. 21. Rudder angles with two rudders stuck ($\xi = 0.5$).

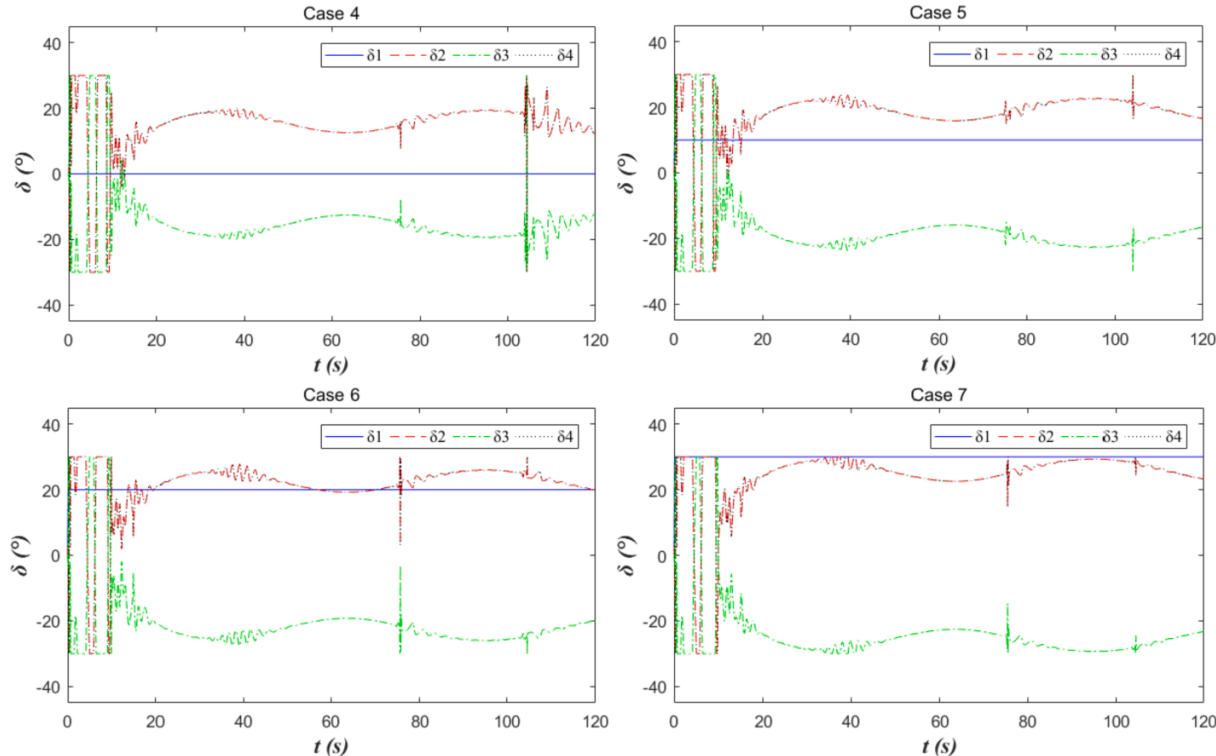


Fig. 19. Rudder allocation with one rudder stuck ($\xi = 0.5$).

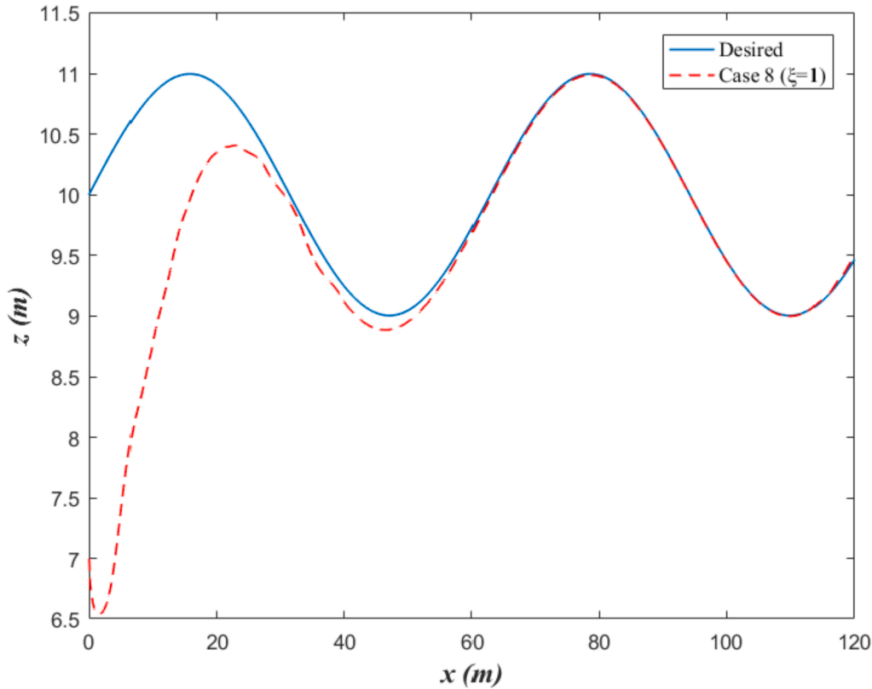


Fig. 22. Trajectory with two rudders stuck ($\xi = 1$).

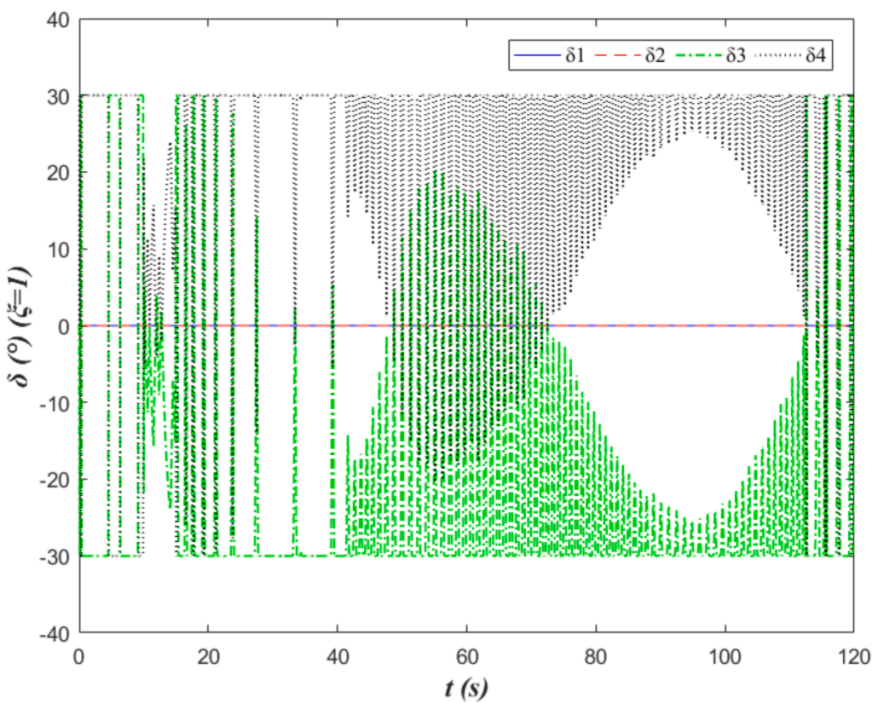


Fig. 23. Rudder angles with two rudders stuck ($\xi = 1$).

4.3. Robust test against different disturbances

To further verify the robust performance of the proposed controller against disturbance, three simulation cases are carried out with different disturbances in this subsection. In case 1, time-varying disturbances are introduced to the system. In case 2, the disturbances are not only time-varying but also state-dependent. In case 3, more complex segmented disturbances are applied. The specific disturbance settings are designed as follows:

$$\begin{aligned} \text{Case 1 : } & \left\{ \begin{array}{l} d_u = 0.01 \sin(0.1t) + 0.01 \\ d_w = 0.01 \cos(0.1t) - 0.01 \\ d_q = 0.01 \sin(0.2t) + 0.01 \end{array} \right. \\ \text{Case 2 : } & \left\{ \begin{array}{l} d_u = 0.03 \sin(0.1t) + 0.03 \cos(0.2t) + 0.03u^2 - 0.01 \\ d_w = 0.03 \sin(0.1t) + 0.03 \cos(0.2t) + 0.03w^2 - 0.01 \\ d_q = 0.03 \cos(0.1t) + 0.03 \sin(0.2t) + 0.03q^2 + 0.01 \end{array} \right. \\ \text{Case 3 : } & \left\{ \begin{array}{ll} \begin{array}{l} d_u = \begin{cases} 0.03 \sin(0.1t - 0.1) & t < 75s \\ 0.03u \cos(0.1t) + 0.04 \sin(0.2t) + 0.03u^2 - 0.03 & t \geq 75s \end{cases} \\ d_w = \begin{cases} 0.03 \sin(0.1t - 0.2) & t < 75s \\ 0.04w \sin(0.1t) + 0.03 \cos(0.2t) - 0.03w^2 - 0.03 & t \geq 75s \end{cases} \\ d_q = \begin{cases} 0.03 \cos(0.1t + 0.1) & t < 75s \\ 0.03q \cos(0.1t) + 0.04 \sin(0.2t) - 0.03q^2 + 0.03 & t \geq 75s \end{cases} \end{array} \end{array} \right. \end{aligned}$$

The desired trajectory and initial conditions of the system are the same as subsection 4.2. The trajectory tracking performance and tracking errors are shown in Fig. 10 and Fig. 11. It can be seen that under the three different kinds of disturbances, the proposed controller can still show good trajectory tracking performance, thus demonstrating good robustness against disturbances. Meanwhile, some fluctuations are observed as the disturbances suddenly changed in case 3, which is normal since the system states have changed and the controller needs some time to adjust. To further distinguish the system robustness against three different kinds of disturbances, data analyses of steady-state tracking errors are shown in Fig. 12, where AVE(.) represents the average value, MAX(.) represents the maximum value, and STDEV(.) denotes the standard deviation value. It is clearly seen that the tracking errors can all maintain at a low level in cases 1–3. However, as the disturbance becomes more complicated, the tracking accuracy is degraded.

The estimations of d_u , d_w , and d_q in three simulation cases are shown in Fig. 13, 14 and 15. The results indicate that the proposed disturbance observer can achieve good estimation with small errors. Besides, since the linear velocities are unmeasured, the disturbance observer has to be designed based on the estimate value of linear velocities rather than the actual values, when there is a deviation between the velocity estimation value and the actual value in the initial adjustment phase, some errors appear in the disturbance observation. This phenomenon is normal and will not affect the overall disturbance observation.

Based on the above analyses, it can be concluded that the proposed method has good disturbance observation ability, thus leading to good robustness against disturbances.

4.4. Robust test against rudder failures

Rudder stuck is a common type of rudder failure, which directly affect maneuverability and may bring great danger to the AUV. The X-rudder AUV discussed in this paper has multi-rudder independent control capability, so it still has certain maneuverability when some rudders are stuck. Moreover, the proposed multi-objective optimization method can still achieve rudder allocation when some rudders are stuck. Therefore, the proposed controller has certain robustness against rudder failures.

In this section, the robustness of proposed controller will be tested against rudder failures, and the adjusting function of parameter ξ will also be verified. The rudder stuck settings are shown in Table 2. In cases 4–7, the condition of one rudder stuck is considered, whereas the condition of two rudders stuck is considered in case 8. The desired trajectory, initial conditions, and disturbance settings of the system are the same as subsection 4.2.

The simulations of this section are implemented in following two stages:

First, the trajectory tracking performance of proposed controller is verified with one rudder stuck in cases 4–7. The weight coefficient of optimization objective function is selected as $\xi = 0.5$, which means both the trajectory tracking and energy consumption problem are considered in optimization objective. The tracking trajectories and tracking errors of cases 4–7 are shown in Fig. 16 and Fig. 17. It is seen that the proposed controller can still achieve good trajectory tracking with one rudder stuck. Although the trajectory tracking errors are different under different rudder stuck angles, they are all maintained at a lower level. To further analyze the tracking performance of proposed controller, more stuck angles are considered across the entire rudder range $[-30^\circ, 30^\circ]$, and the simulation results are shown in Fig. 18. It is observed that the proposed controller can achieve satisfactory trajectory tracking with small errors under all the rudder stuck samples. The rudder allocation performances of cases 4–7 are shown in Fig. 19. Compared with section 4.2, the rudder angles exhibit more dramatic changes. Therefore, it is proved that the proposed controller can achieve good trajectory tracking with one rudder stuck, but other rudders have to be controlled more

intensely to make up for the impact of stuck rudder.

Second, the trajectory tracking performance of proposed controller is verified under the condition of two rudders stuck. When $\xi = 0.5$, the tracking trajectory and rudder allocation of case 8 are shown in Fig. 20 and Fig. 21. Compared with cases 4–7, it is easily observed that the trajectory tracking performance of case 8 is degraded when trajectory tracking and energy consumption problem are both considered in optimization objective. Besides, as shown in Fig. 21, since the two rudders have been stuck, the rudder angles of the other two rudders show dramatic changes in order to achieve the control target. To further verify the adjusting function of parameter ξ , the energy consumption problem is ignored and the value of ξ is changed to $\xi = 1$. The simulation results are shown in Fig. 22 and Fig. 23. It is clearly seen that the tracking performance of case 8 is greatly improved when energy consumption problem is ignored. But as shown in Fig. 23, this also has some negative effects, that is, the rudder angles change more drastically, thus consuming too much energy.

From the above simulation results, following conclusions can be drawn:

- 1) The proposed multi-objective optimization method has certain robustness against rudder failures, and can achieve good trajectory tracking with one rudder stuck. However, when facing with serious failures, the maneuverability and trajectory tracking capability will be degraded.
- 2) When facing with two rudders stuck, the tracking performance can be improved by adjusting the optimization target, but it brings huge energy consumption. Moreover, too aggressive rudder angle control may not be realized under real working conditions.
- 3) When facing with most serious rudder failures such as three rudders stuck, the maneuverability will be degraded more seriously, which may cause failed tracking missions. In this case, the trajectory tracking mission needs to be adjusted, or even the vehicle should be recycled.

Based on the above analysis, we believe that in the presence of rudder failures, it is better to have a failure analyzer to classify the failures, and then take corresponding methods based on the result of the failure quantification: for example, when facing with low-level failure, the optimization target or control parameters can be adjusted to help complete the mission, whereas when facing with high-level failure, it is preferred to change the tracking target or perform emergency recycling. The simulation results of this paper will provide a good basis for the design of the rudder failure analyzer.

In addition, this paper only analyzes the tracking control in the vertical plane. In fact, the impact of the rudder failure on the vehicle is multi-faceted. Even if the tracking control can be completed in the vertical plane, the control of the horizontal plane may suffer from other negative effects. This will be addressed in our future works.

5. Conclusions

This paper addresses the trajectory tracking problem of a X-rudder AUV in vertical plane subjects to velocity sensor failure and uncertainties. An optimal robust trajectory tracking controller is developed based on linear velocity observers, LOS based backstepping kinematics controller, robust disturbance rejection dynamics controller, and multi-objective optimal rudder allocator. The salient features of the proposed control method are as follows. First, the unmeasured linear velocities can be well estimated by ESOs, which helps releasing the requirements of linear velocity measurement. Second, the system robustness is addressed by the proposed robust disturbance rejection dynamics controller. Third, the multi-objective optimal rudder allocator can achieve satisfactory rudder angle calculation with rudder input saturation, and it is not only energy efficient but also robust against rudder failures. Lyapunov analysis is performed to prove the stability and performance

of the proposed controller. Moreover, the robustness and effectiveness of the controller are tested and validated through comparative numerical simulations. For future research, it is of interest to extend the current work to 3D space and incorporate more state constraints and fault tolerant methods in the trajectory tracking controller design.

Author contribution statement

1. Yingkai Xia: Conceptualization, Methodology, Software, Validation, Writing - Original Draft, Visualization;
2. Kan Xu: Investigation, Data curation, Software;
3. Wenjin Wang: Data curation, Validation;
4. Guohua Xu: Conceptualization, Supervision;
5. Xianbo Xiang: Writing- Reviewing and Editing;
6. Ye Li: Writing- Reviewing and Editing.

Declaration of competing interest

The authors declare that they have no known competing financial interests or personal relationships that could have appeared to influence the work reported in this paper.

Acknowledgement

This work was supported in part by National Natural Science Foundation of China [grant numbers 51479114, 51579111, 51761135012], and the post-doctoral foundation of China [grant number 2018M632117].

References

- Al Makdah, A.A.R., Daher, N., Asmar, D., Shamma, E., 2019. Three-dimensional trajectory tracking of a hybrid autonomous underwater vehicle in the presence of underwater current. *Ocean Eng.* 185, 115–132.
- Chen, L., Cui, R., Yang, C., Yan, W., 2019. Adaptive neural network control of underactuated surface vessels with guaranteed transient performance: theory and experimental results. *IEEE Trans. Ind. Electron.* <https://doi.org/10.1109/TIE.2019.2914631>.
- Chu, Z.Z., Xiang, X.B., Zhu, D.Q., Luo, C.M., Xie, D., 2018. Adaptive fuzzy sliding mode diving control for autonomous underwater vehicle with input constraint. *Int. J. Fuzzy Syst.* 20 (5), 1460–1469.
- Cui, R.X., Yang, C.G., Li, Y., Sharma, S., 2017. Adaptive neural network control of AUVs with control input nonlinearities using reinforcement learning. *IEEE Trans. Syst. Man Cybern. Syst.* 47 (6), 1019–1029.
- Cui, R.X., Zhang, X., Cui, D., 2016. Adaptive sliding-mode attitude control for autonomous underwater vehicles with input nonlinearities. *Ocean Eng.* 123, 45–54.
- Guo, Y., Qin, H., Xu, B., et al., 2019. Composite learning adaptive sliding mode control for AUV target tracking. *Neurocomputing* 351, 180–186.
- Li, B., Qin, K., Xiao, B., et al., 2019. Finite-time Extended State Observer based fault tolerant output feedback control for attitude stabilization. *ISA (Instrum. Soc. Am.) Trans.* <https://doi.org/10.1016/j.isatra.2019.01.039>.
- Li, H., Yan, W., 2017. Model predictive stabilization of constrained underactuated autonomous underwater vehicles with guaranteed feasibility and stability. *IEEE ASME Trans. Mechatron.* 22 (3), 1185–1194.
- Li, Y., Cui, R., Li, Z., Xu, D., 2018. Neural network approximation-based near-optimal motion planning with kinodynamic constraints using RRT. *IEEE Trans. Ind. Electron.* 65 (11), 8718–8729.
- Liu, L., Wang, D., Peng, Z.H., 2019. State recovery and disturbance estimation of unmanned surface vehicles based on nonlinear extended state observers. *Ocean Eng.* 171, 625–632.
- Miao, J., Wang, S., Tomovic, M.M., Zhao, Z., 2017. Compound line-of-sight nonlinear path following control of underactuated marine vehicles exposed to wind, waves, and ocean currents. *Nonlinear Dyn.* 89 (4), 2441–2459.
- Naik, M.S., Singh, S.N., 2007. State-dependent Riccati equation-based robust dive plane control of AUV with control constraints. *Ocean Eng.* 34 (11), 1711–1723.
- Peng, Z.H., Wang, J., 2018. Output-feedback path-following control of autonomous underwater vehicles based on an extended state observer and projection neural networks. *IEEE Trans. Syst. Man Cybern.: Off. Syst.* 48 (4), 535–544.
- Peng, Z.H., Wang, J., Han, Q.L., 2019. Path-following control of autonomous underwater vehicles subject to velocity and input constraints via neurodynamic optimization. *IEEE Trans. Ind. Electron.* 66 (11), 8724–8732.
- Qiao, L., Yi, B.W., Wu, D.F., Zhang, W.D., 2017. Design of three exponentially convergent robust controllers for the trajectory tracking of autonomous underwater vehicles. *Ocean Eng.* 134, 157–172.
- Qiao, L., Zhang, W.D., 2017. Adaptive non-singular integral terminal sliding mode tracking control for autonomous underwater vehicles. *IET Control Theory & Appl.* 11 (8), 1293–1306.

- Qiao, L., Zhang, W.D., 2019. Adaptive second-order fast nonsingular terminal sliding mode tracking control for fully actuated autonomous underwater vehicles. *IEEE J. Ocean. Eng.* 44 (2), 363–385.
- Sarhadi, P., Noei, A., Khosravi, A., 2016. Adaptive integral feedback controller for pitch and yaw channels of an AUV with actuator saturations. *ISA Trans.* 65, 284–295.
- Shojaei, K., Dolatshahi, M., 2017. Line-of-sight target tracking control of underactuated autonomous underwater vehicles. *Ocean. Eng.* 133, 244–252.
- Shen, C., Shi, Y., Buckingham, B., 2018. Trajectory tracking control of an autonomous underwater vehicle using Lyapunov-based model predictive control. *IEEE Trans. Ind. Electron.* 65 (7), 5796–5805.
- von Ellenrieder, K.D., 2019. Dynamic surface control of trajectory tracking marine vehicles with actuator magnitude and rate limits. *Automatica* 105, 433–442.
- Van, M., 2019. An enhanced tracking control of marine surface vessels based on adaptive integral sliding mode control and disturbance observer. *ISA Trans.* 90, 30–40.
- Wang, H.Q., Chen, B., Lin, C., 2013. Direct adaptive neural tracking control for a class of stochastic pure-feedback nonlinear systems with unknown dead-zone. *Int. J. Adapt. Control Signal Process.* 27, 302–322.
- Wang, N., Sun, Z., Su, S.-F., Wang, Y., 2018. Fuzzy uncertainty observer-based path following control of underactuated marine vehicles with unmodeled dynamics and disturbances. *Int. J. Fuzzy Syst.* 20 (8), 2593–2604. <https://doi.org/10.1007/s40815-018-0522-3>.
- Wynn, R.B., Huvenne, V.A.I., Bas, T.P.L., et al., 2014. Autonomous underwater vehicles (AUVs): their past, present and future contributions to the advancement of marine geoscience. *Mar. Geol.* 352 (2), 451–468.
- Xia, Y.K., Xu, K., Li, Y., Xu, G.H., Xiang, X.B., 2019a. Improved line-of-sight trajectory tracking control of under-actuated AUV subjects to ocean currents and input saturation. *Ocean. Eng.* 174, 14–30.
- Xia, Y.K., Xu, K., Li, Y., et al., 2019b. Adaptive trajectory tracking control of a cable-driven underwater vehicle on a tension leg platform. *IEEE Access* 7 (1), 35512–35531.
- Xiao, H., Cui, R., Xu, D., 2018. A sampling-based Bayesian approach for cooperative multi-agent online search with resource constraints. *IEEE Trans. Cybern.* 48 (6), 1773–1785.
- Xu, J., Wang, M., Qiao, L., 2015. Dynamical sliding mode control for the trajectory tracking of underactuated unmanned underwater vehicles. *Ocean. Eng.* 105, 54–63.
- Yu, C.Y., Liu, C.H., Lian, L., Xiang, X.B., Zeng, Z., 2019b. ELOS-based path following control for underactuated surface vehicles with actuator dynamics. *Ocean. Eng.* 187, 106139.
- Yu, C.Y., Xiang, X.B., Lapierre, L., Zhang, Q., 2018. Robust magnetic tracking of subsea cable by AUV in the presence of sensor noise and ocean currents. *IEEE J. Ocean. Eng.* 43 (2), 311–322.
- Yu, C.Y., Xiang, X.B., Wilson, P.A., Zhang, Q., 2019a. Guidance-error-based robust fuzzy adaptive control for bottom following of a flight-style AUV with saturated actuator dynamics. *IEEE Trans. Cybern.* <https://doi.org/10.1109/TCYB.2018.2890582>.
- Zhang, F., Marani, G., Smith, R.N., Choi, H.T., 2015. Future trends in marine robotics. *IEEE Robot. Autom. Mag.* 22 (1), 14–21 122.
- Zhang, Q., Zhang, J.L., Chemori, A., Xiang, X.B., 2018a. Virtual submerged floating operational system for robotic manipulation. *Complexity* 1–18. <https://doi.org/10.1155/2018/9528313>. 2018.
- Zhang, W., Teng, Y., Wei, S., et al., 2018b. The robust H-infinity control of UUV with Riccati equation solution interpolation. *Ocean. Eng.* 156, 252–262.
- Zhang, Y.H., Li, Y.M., Sun, Y.S., Zeng, J.F., Wan, L., 2017. Design and simulation of X-rudder AUV's motion control. *Ocean. Eng.* 137, 204–214.
- Zhang, Y.D., Liu, X.F., Luo, M.Z., Yang, C.G., 2019. MPC-based 3-D trajectory tracking for an autonomous underwater vehicle with constraints in complex ocean environments. *Ocean. Eng.* 189, 106309.
- Zheng, Z., Huang, Y., Xie, L., Zhu, B., 2017. Adaptive trajectory tracking control of a fully actuated surface vessel with asymmetrically constrained input and output. *IEEE Trans. Control Syst. Technol.* <https://doi.org/10.1109/TCST.2017.2728518>.
- Zheng, Z., Sun, L., 2016. Path following control for marine surface vessel with uncertainties and input saturation. *Neurocomputing* 177, 158–167.